

TeZO: Empowering the Low-Rankness on the Temporal Dimension in the Zeroth-Order Optimization for Fine-tuning LLMs

Yan Sun¹ Tiansheng Huang Liang Ding¹ Li Shen² Dacheng Tao³

Abstract

Zeroth-order optimization (ZO) has demonstrated remarkable promise in efficient fine-tuning tasks for Large Language Models (LLMs). In particular, recent advances incorporate the low-rankness of gradients, introducing low-rank ZO estimators to further reduce GPU memory consumption. However, most existing works focus solely on the low-rankness of each individual gradient, overlooking a broader property shared by all gradients throughout the training, i.e., all gradients approximately reside within a similar subspace. In this paper, we consider two factors together and propose a novel low-rank ZO estimator, TeZO, which captures the low-rankness across both the model and temporal dimension. Specifically, we represent ZO perturbations along the temporal dimension as a 3D tensor and employ Canonical Polyadic Decomposition (CPD) to extract each low-rank 2D matrix, significantly reducing the training cost. TeZO can also be easily extended to the Adam variant while consuming less memory than MeZO-SGD, and requiring about only 35% memory of MeZO-Adam. Both comprehensive theoretical analysis and extensive experimental research have validated its efficiency, achieving SOTA-comparable results with lower overhead of time and memory.

1. Introduction

As the model size progresses at an extraordinary rate (Zhang et al., 2022; Touvron et al., 2023; Achiam et al., 2023), memory and computational resources have become the primary bottleneck limiting development. In response to this challenge, ZO has opened up new possibilities for efficient training (Shen et al., 2023). Adopting gradient-free updates with

a small amount of high-quality data perfectly unlocks the knowledge of the entire domain, offering significant potential for several practical applications. Since Spall (1992) introduced ZO as a promising alternative to FO in the training process, it has been widely applied in gradient-computation-challenged scenarios (Wang et al., 2018; Liu et al., 2020) and in black-box optimization (Chen et al., 2017; Tu et al., 2019). Recent studies have also highlighted the great potential of ZO in fine-tuning LLMs. Malladi et al. (2023) propose the MeZO method which adopts classical ZO-SGD (Ghadimi & Lan, 2013) for fine-tuning. Furthermore, it reduces memory costs by only preserving random seeds instead of variables. Compared to FO, it can achieve comparable performance while requiring approximately 10% of memory in practice, greatly improving memory efficiency.

Although ZO has made significant progress, it still faces two main challenges, i.e., i) lack of detailed characterization of gradients; ii) the costs of optimization states to generate random variables significantly increase as d grows. This also highlights the bottleneck of ZO methods in LLM tasks. Recent advances learned the strong low-rank nature of gradients in LLMs (Wang et al., 2023; Jaiswal et al., 2024), making low-rank representations in ZO methods as an ingenious solution to the aforementioned issues. With barely compromising performance, low-rank ZO methods effectively reduce the required memory for ZO estimations from $\mathcal{O}(d)$ to $\mathcal{O}(\sqrt{dr})$ at most, where r is the rankness constant (Chen et al., 2024; Yu et al., 2024). This implementation further endows the ZO method with superior value in the tasks of fine-tuning LLMs. Nonetheless, this technique still exhibits substantial potential for further developments.

Our Motivations. Existing methods only consider each individual gradient to be low-rank. From the entire training perspective, the total cost achieves $\mathcal{O}(\sqrt{dT})$ after T iterations. Although techniques like lazy updates reduce the frequency of generating factor vectors, training costs still expand linearly with \sqrt{d} . It indicates that merely considering the low-rank form of each individual gradient is insufficient. This inspires our contemplation: *could the low-rankness be incorporated along the temporal dimension as well?*

To investigate an efficient approach to addressing this question, in this paper, we comprehensively study the character-

¹Faculty of Engineering, The University of Sydney ²School of Cyber Science and Technology, Shenzhen Campus of Sun Yat-sen University ³The college of Computing & Data Science, Nanyang Technological University. Correspondence to: Li Shen <mathshenli@gmail.com>.

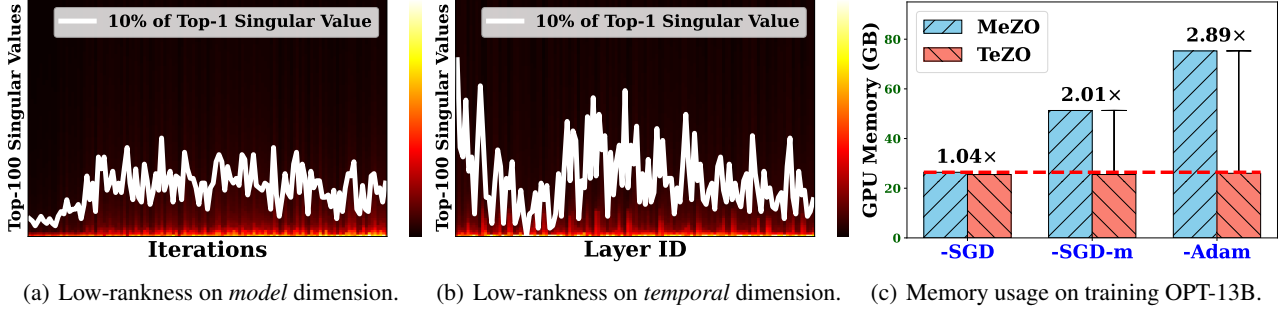


Figure 1. (a) and (b) are validation of the low-rankness of gradients. We fine-tune OPT-1.3B on SST-2 and calculate top-100 singular values of gradients of `layers.9.self_attn.out_proj.weight`. We then concatenate these singular value vectors and display them as a heat-map in (a). Then we concatenate the normalized gradient of each layer over a total of T iterations into a matrix with the size of $d_l \times T$, calculate the top-100 singular values corresponding to layers and display them as a heat-map in (b). In (c), we record the GPU memory usage of MeZO, our TeZO, and corresponding variants on training OPT-13B model. We also provide more interesting experiments on the low-rankness and studies of subspace of gradients on LLaMA-7B in Appendix A.1.

istics of the gradients in LLMs. As shown in Figure 1.(a) and (b), in the tasks of fine-tuning LLMs, the gradients exhibit the following two properties simultaneously: i) the individual gradient at each iteration is approximately low-rank; ii) all gradients along T iterations lie almost within a similar subspace. Obviously, combining properties i) and ii) can lead to higher efficiency. Inspired by this, we propose the TeZO estimator to empower the low-rankness on the temporal dimension. Specifically, we estimate the ZO perturbations as a 3D tensor with the size of $m \times n \times T$. By adopting the Canonical Polyadic Decomposition (CPD) (Hitchcock, 1927), the 3D tensor can be estimated by the sum of r rank-1 tensors where r approximates its rank. The joint low-rankness significantly reduces the cost of factor vectors during computation. At each iteration t , we only need to generate temporal factor vector to extract a 2D matrix, further lowering the costs from $\mathcal{O}(\sqrt{d}T)$ to $\mathcal{O}(\sqrt{d} + T)$. We also introduce an auxiliary technique to dynamically select the rank r_l for each layer. In addition, we propose both memory-efficient momentum-based and adaptivity-based variants, i.e. TeZO-m and TeZO-Adam, which demonstrate the high scalability of the TeZO method. As shown in Figure 1.(c), TeZO-Adam consumes less memory than MeZO-SGD, and requiring about only 35% memory of MeZO-Adam. Both comprehensive theoretical analysis and extensive experimental research are conducted to validate its efficiency. TeZO-Adam achieves performance superior to MeZO-Adam and other ZO optimizers, while requiring only the memory overhead of general ZO-SGD. We summarize our contributions as follows:

- By jointly considering low-rankness of gradients and their similarity on LLMs, we propose a novel low-rank ZO estimator, TeZO, which constructs the ZO perturbations via CPD to reduce the training overhead.
- We introduce an auxiliary technique to dynamically

select the rank for each layer and extend TeZO to two memory-efficient variants, TeZO-m and TeZO-Adam. Both require lower memory consumption and time cost than MeZO-SGD and significantly lower than the costs of corresponding variants in MeZO.

- We prove that TeZO is an unbiased estimator of FO gradient, maintaining the comparable variance and convergence rate as existing ZO methods with less overhead. Extensive experiments are conducted to validate its fine-tuning efficiency on LLMs.

2. Related Work

Zero-Order Optimization. Since Spall (1992) proposed the ZO method, it has been extensively studied and practically incorporated in various domains (Chen et al., 2017; Tu et al., 2019; Vemula et al., 2019; Hajinezhad et al., 2019; Gratton et al., 2021). By avoiding the massive computation and memory requirements of BP, it significantly reduces the training cost while maintaining high performance. As an alternative to FO, it has also been widely explored from several optimization perspectives, e.g. convergence for convex and non-convex (Wang et al., 2018; Golovin et al., 2019; Cheng et al., 2021), non-smooth (Liu et al., 2018a; Kazemi & Wang, 2024; Rando et al., 2024), variance reduction (Liu et al., 2018b; Ji et al., 2019) and primal dual methods (Liu et al., 2018a; Yi et al., 2021; Huang et al., 2024). It has also demonstrated strong potential for applications in certain practical scenarios, e.g. attack and defense (Zhao et al., 2020; Kariyappa et al., 2021), privacy protection (Gratton et al., 2021; Zhang et al., 2023; Gupta et al.), fairness (Chen et al., 2023; Wang et al., 2024b), multi-agent (Tang et al., 2020; Maritan & Schenato, 2023), and efficient training (Nikolakakis et al., 2022; Fang et al., 2022; Mukhoty et al., 2023). These developments highlight the powerful potential of ZO methods in deep learning and artificial intelligence.

Fine-tuning LLMs with ZO. In this paper, we focus on the tasks of fine-tuning LLMs. Recent research on LLMs has demonstrated their immense value (Brown et al., 2020; Kojima et al., 2022). However, expensive time and memory costs in the training have become a significant barrier and hinder the research and application (Zhao et al., 2023; Naveed et al., 2023). To unlock the tremendous potential of LLMs, researchers focus more on the training efficiency, leading to significant progress. The application of ZO optimizers has become a shining star from an optimization perspective. Since Malladi et al. (2023) introduce the MeZO method, a series of ZO optimizer variants have been widely developed. Jiang et al. (2024); Yang et al. (2024); Zhao et al. (2024c;a) focus on incorporating adaptivity and curvature information to accelerate ZO optimizers for LLMs. Liu et al. (2024); Guo et al. (2024); Wang et al. (2024a) incorporate the sparsity to further reduce the calculations. Gautam et al. (2024) expand the variance reduction ZO estimator and evaluate its improvements in fine-tuning LLMs. These methods improve ZO methods from the general optimization perspective, yield additional computational and memory overhead. Recently, Yu et al. (2024); Chen et al. (2024) further learn the low-rankness of each single gradient and propose different low-rank ZO estimators. These insightful works have advanced the application of ZO in fine-tuning LLMs.

Our work. Existing works focus on improving the calculation on single-step ZO gradient individually, ignoring the low-rankness in the gradient subspace. Our work extends this in the ZO estimator and achieves higher efficiency.

3. Preliminaries

In this section, we introduce notations and review developments of ZO and its recent advances in fine-tuning LLMs.

Notations. We use lowercase letters to represent 1D vectors, e.g. z , uppercase letters to represent 2D matrices, e.g. Z , and bold uppercase letters to represent 3D tensors, e.g. \mathbf{Z} . Scalars are represented as lowercase Greek letters, e.g. α . Other special computation symbols will be introduced in detail when they are first mentioned. Table 1 shows some specific notation adopted in this paper.

Table 1. Some notations adopted in the context.

Symbol	Notations
w / W	learnable parameters
$f(\cdot)$	the general objective in the training
$\nabla f(w)$	FO gradient w.r.t. w
$\nabla^0 f(w)$	ZO gradient w.r.t. w
r	rank value for the ZO perturbation
η	global learning rate / step size
ρ	perturbation rate in the ZO estimation

ZO Optimizer. We consider the general and classical minimization problem on the task of fine-tuning LLMs:

$$\min_w f(w) \triangleq \mathbb{E}_{\xi \sim \mathcal{D}} [f(w, \xi)], \quad (1)$$

where $w \in \mathbb{R}^d$ is the learnable parameters and ξ is the fine-tuning dataset sampled from the distribution \mathcal{D} . In this paper, we focus on a classical and widely adopted ZO method, *Simultaneous Perturbation Stochastic Approximation* (SPSA) (Spall, 1992). Specifically, SPSA estimates ZO gradient as:

$$\nabla^0 f(w, \xi) = \frac{f(w + \rho z, \xi) - f(w - \rho z, \xi)}{2\rho} z, \quad (2)$$

where $z \sim \mathcal{N}(0, I_d)$ is a random variable and ρ is the perturbation rate. The estimation precision highly depends on the selection of the perturbation ρ . When ρ is small enough, Eq.(2) achieves an unbiased estimate of the FO gradient and efficiently drives the training process. Through two forward passes, it measures the projection component of the true gradient in the direction of the random variable z .

Fine-tuning LLMs with ZO. MeZO (Malladi et al., 2023) explores the tremendous potential of ZO methods in fine-tuning LLMs. Moreover, to reduce memory usage, it leverages PyTorch’s permutation feature in random libs, replacing the storage of all random variables by recording the initial random seed for each iteration, namely the *resampling technique*. This implementation enables the ZO method to achieve up to a $12\times$ memory saving in fine-tuning LLMs. The simple ZO-SGD method is sufficient to achieve performance comparable to FO methods in most tasks, enabling the training of ultra-large models like OPT-13B to be efficiently carried out on just a single A100 device. This has significantly advanced research in fine-tuning LLMs.

Low-rank ZO. Generally speaking, the parameter dimension of LLMs is extremely large, which constitutes a new bottleneck for the further development of MeZO: training costs of the ZO gradients increase linearly with the model dimension d . Furthermore, an important fact in fine-tuning LLMs is also ignored: the low-rankness of the gradients. Therefore, the applications of low-rank ZO techniques have emerged. Chen et al. (2024) propose to apply matrix factorization as $Z = UV^\top$ ($Z \in \mathbb{R}^{m \times n}$, $U \in \mathbb{R}^{m \times r}$, $V \in \mathbb{R}^{n \times r}$). Additionally, Yu et al. (2024) adopt the form $Z = U\Sigma V^\top$ where $\Sigma \in \mathbb{R}^{r \times r}$, as shown in Figure 2. These techniques estimate the low-rank form of each individual perturbation per iteration, reducing the training cost of the ZO method in fine-tuning LLMs. Inspired by these insightful works, we examine another important aspect that is overlooked in the designs of previous works, i.e., low-rankness on the temporal dimension. Through the joint low-rank estimation, we propose the TeZO method which can further improve the efficiency of the ZO method in fine-tuning LLMs. Further discussions are provided in the next section.

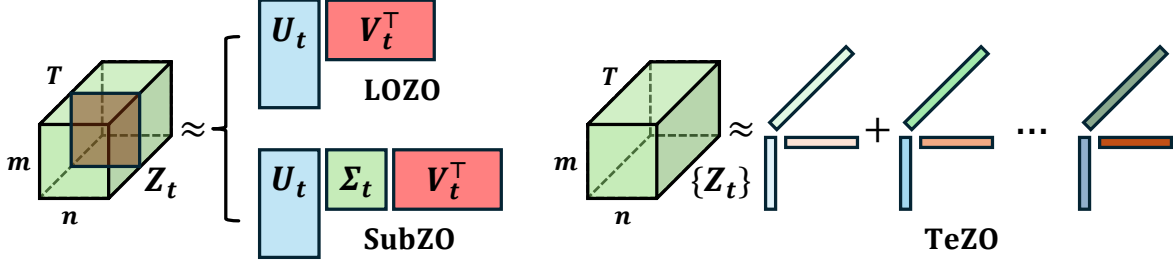


Figure 2. The ZO diagrams for LOZO, SubZO, and our TeZO method. LOZO and SubZO focus on estimating a single perturbation Z_t as the product of low-rank matrices. TeZO construct the entire perturbation set $Z = \{Z_t\}$ via the CPD in the 3D tensor.

4. Methodology

In this section, we introduce our proposed TeZO method. Then we introduce the adaptive selection of the rank of layer-wise gradients. Finally, we present the momentum-based and adaptivity-based extensions of the TeZO method.

4.1. Canonical Polyadic Decomposition and TeZO

Canonical Polyadic Decomposition (Hitchcock, 1927), also known as *Parallel Factor Analysis*, is the tensor decomposition technique widely used in data analysis, signal processing, and machine learning. It is a generalization of matrix factorization to higher-order tensors (multi-dimensional arrays). CPD aims to decompose a 3D tensor $Z \in \mathbb{R}^{m \times n \times T}$ into a sum of rank-one tensors and each rank-one tensor is expressed as the outer product of vectors:

$$Z \approx \sum_{s=1}^r \chi_s \circ u_s \circ v_s, \quad (3)$$

$$\text{where } Z_t \approx \sum_{s=1}^r \tau_s \cdot (u_s \circ v_s),$$

where $\tau_s = (\chi_s)_t$ at time t and \circ denotes the outer product. $\chi_s \in \mathbb{R}^T$, $u_s \in \mathbb{R}^m$, $v_s \in \mathbb{R}^n$ are three factor vectors.

Based on understanding the low-rank nature along the temporal dimension, we propose a novel low-rank estimation approach to represent the gradient perturbation variables at each iteration, as outlined in Eq.(3). In LLMs, the pro-

portion of 2D model parameters is much larger than that of 1D parameters, so we primarily consider the 2D cases. Specifically, in addition to the conventional factor vectors u and v for the model dimensions, we introduce the factor vectors χ for the temporal dimension. These three dimensions are independent of each other. Both u and v can be initialized at the beginning of training. Therefore, in the t -th iteration, we only need information related to the variable τ_s without any additional redundant variables, which can still significantly reduce training costs. Compared to existing studies, we summarize the results in Table 2.

4.2. Layer-wise Selection of the Rank r

The selection of rank r remains an open challenge. Since ZO methods are typically employed in scenarios where FO gradients are unavailable, it is difficult to directly determine the precise rank of gradients. Recent studies have emphasized the feasibility of low-rank structures, and the rank r is empirically treated as a constant hyperparameter. In fact, r essentially represents a trade-off between performance and efficiency, and selecting an appropriate value for r can significantly enhance the balance between these two factors. Although the constant selection can yield reliable performance, our goal is to identify a more refined solution.

To comprehensively study the rank r , we learn its potential connection to the model parameters in this paper. Furthermore, based on this understanding, we dynamically select the rank on different layers in the TeZO method. We consider the general cascade neural network as following:

$$X_l = \sigma_l(A_l), \quad A_l = W_l X_{l-1} + b_l, \quad (4)$$

where $\sigma_l(\cdot)$ is activation function, $l \leq L$ is the index of each layer, W_l and B_l are the weight and bias of the l -th layer. Let the final output simply be X_L , therefore, we can calculate the gradient of the parameters W_l as:

$$\frac{\partial f}{\partial W_l} = \left(\prod_{p=l+1}^L W_p \right)^\top \partial \Phi(\sigma_L, \sigma_{L-1}, \dots, \sigma_l), \quad (5)$$

Table 2. The number of the sampled elements for training a 2D weight ($m \times n = d$) after T iterations with the corresponding ZO.

Method	Total elements of generating	Optimal
MeZO	mnT	$\mathcal{O}(d \cdot T)$
SubZO	$(m + n + r)rT$	$\mathcal{O}(\sqrt{d} \cdot T)$
LOZO	$(m + n)rT$	$\mathcal{O}(\sqrt{d} \cdot T)$
TeZO	$(m + n + T)r$	$\mathcal{O}(\sqrt{d} + T)$

where $\partial\Phi(\cdot)$ are the joint gradients for all activations from the total mini-batch data samples, whose rank is closely related to the similarity of the input data. In this paper, we focus on the impact from model parameters. According to the rank propagation, the rankness of each gradient satisfies:

$$\begin{aligned} \text{Rank}\left(\frac{\partial f}{\partial W_l}\right) &\leq \text{Rank}\left(\prod_{p=l+1}^L W_p\right) \\ &\leq \min(\text{Rank}(W_{l+1}), \dots, \text{Rank}(W_L)). \end{aligned} \quad (6)$$

Typically, during training, due to the use of weight decay regularization, the model parameters tend to maintain a high degree of low-rankness. Therefore, the gradients also inherit this property, meaning that the low-rankness of the gradients originates from the low-rankness of the model parameters. We adaptively determine the rank of different layers based on the insight from Eq.(6). In LLMs, there is a natural cascade block structure, where each block contains components such as the attention module and the feed-forward network (FFN) module. We adopt the truncated Eq.(6) to estimate the rankness of each layer within a block. Specifically, we split L into B blocks as $[\{l_0\}, \{l_1\}, \dots, \{l_B\}]$ where $\sum_b l_b = L$. The rankness of the gradient of the l -th layer will be estimated as follows:

$$r_l = \min(\{\text{Rank}(W_{\{l_b\}})\}, r_{max}), \quad (7)$$

where $l \in \{l_b\}$ and r_{max} is a constant. Eq.(7) is designed to preserve the transitivity of such estimations on the rankness, ensuring that the estimated r does not become excessively low due to very large L . $\text{Rank}(W)$ is defined as the index of the top- r singular values of the matrix W . The selection criterion can be based on the proportion of total energy of singular values or the percentage of the largest singular value to represent its low-rank property. In our experiments, we uniformly set a specific threshold to determine r that those singular values are larger than that threshold. Through Eq.(7), TeZO enables the estimation of the rank of FO gradients without explicitly calculating the FO gradients.

4.3. Applications in General Optimizers

In this part, we mainly introduce the application of TeZO in several classical optimizers, as shown in Algorithm 1.

TeZO. ZO-SGD always serves as a foundational approach in previous works. Similarly, we adopt the resampling technique proposed by MeZO to reduce memory usage. Before each iteration, the random seed is reset to ensure sampling the same variables. Through three perturbations, we can calculate the positive and negative terms, i.e., $f_+ = f(w + \rho z, \xi)$ and $f_- = f(w - \rho z, \xi)$ in Eq.(2), and update the projected coefficient $\kappa = (f_+ - f_-)/2\rho$. It naturally requires only estimating the current Z_t and then performing the update as a general ZO step.

Algorithm 1 TeZO/TeZO-m/TeZO-Adam Methods

Input: model $\{W_l\}$, perturbation rate ρ , learning rate η_l , iterations T , momentum coefficient $\beta_1 = 0.9$, second-order momentum coefficient $\beta_2 = 0.99$, smoothing term $\epsilon = 1e - 5$.

Output: model $\{W_l\}$.

```

1: Initialize the rank list  $[r_1, \dots, r_L]$  via Eq.(7)
2: Initialize the factor vectors  $\{u_s\}$  and  $\{v_s\}$  by layers
3: for  $t = 0, 1, 2, \dots, T - 1$  do
4:   select the minibatch  $\xi_t$  and random seed  $\zeta_t$ 
5:    $W = \text{Perturbation}(W, \rho, \zeta_t)$ ,  $f_+ = f(W, \xi)$ 
6:    $W = \text{Perturbation}(W, -2\rho, \zeta_t)$ ,  $f_- = f(W, \xi)$ 
7:    $W = \text{Perturbation}(W, \rho, \zeta_t)$ ,  $\kappa_t = (f_+ - f_-)/2\rho$ 
8:   reset the random seed as  $\zeta_t$ 
9:   for  $W_l \in W$  do
10:    sample  $\tau \sim \mathcal{N}(0, I_{r_l})$ 
11:    (TeZO)  $G_t = \sum_{s=1}^{r_l} \kappa_t \tau_s \cdot (u_s \circ v_s)$ 
12:    (TeZO-m)  $\tau_M = \beta_1 \tau_M + (1 - \beta_1) \kappa_t \tau$ 
13:     $G_t = \sum_{s=1}^{r_l} (\tau_M)_s \cdot (u_s \circ v_s)$ 
14:    (TeZO-Adam)  $\tau_M = \beta_1 \tau_M + (1 - \beta_1) \kappa_t \tau$ 
15:     $\tau_V = \beta_2 \tau_V + (1 - \beta_2) \kappa_t^2 \tau^2$ 
16:     $M_t = \sum_{s=1}^{r_l} (\tau_M)_s \cdot (u_s \circ v_s)$ 
17:     $V_t = \sum_{s=1}^{r_l} (\tau_V)_s \cdot (u_s^2 \circ v_s^2)$ 
18:     $G_t = M_t / \sqrt{V_t + \epsilon}$ 
19:     $W_l = W_l - \eta_l G_t$ 
20:   end for
21: end for
22: Function Perturbation( $W, \rho, \zeta$ ):
23:   reset the random seed as  $\zeta$ 
24:   for  $W_l \in W$  do
25:    sample  $\tau \sim \mathcal{N}(0, I_{r_l})$ ,  $Z_t = \sum_{s=1}^{r_l} \tau_s \cdot (u_s \circ v_s)$ 
26:     $W_l = W_l + \rho Z_t$ 
27:   end for
```

TeZO-m. SGD-m method has also received widespread attention. The use of momentum allows this method to maintain greater stability during practical training. For the MeZO method, the momentum term requires an additional doubling of parameter storage, which undoubtedly increases the algorithm's cost. However, in the proposed TeZO method, this implementation becomes highly memory-efficient. Specifically, since the factor vectors of the dimensions are not affected by time, the momentum accumulation of Z_t can be equivalently achieved by first applying momentum accumulation to $\kappa_t \tau_t$ and then computing the momentum term. TeZO achieves the global momentum updates with only additional storage of τ_M and is not affected by the model dimension d in the training process.

TeZO-Adam. Adam is highly favored by researchers and demonstrates greater potential in training LLMs. Second-order momentum effectively scales the updates of coordinates with larger long-term changes in the gradient, allow-

ing the model to adaptively adjust the learning rate for each coordinate, thus enabling efficient training. Clearly, the drawback is that it introduces more computational and storage demands. To strictly implement Adam for TeZO, we also face the storage issue of second-order momentum. To reduce the overhead, we propose a *lightweight* variant where the second-order momentum is first computed separately along each factor vector and then merged, thus avoiding significant additional storage. Specifically, we review the squared gradient in second-order momentum for a 2D parameters W_l on the l -th layer in our TeZO method :

$$\begin{aligned} [\nabla^0 f(W_l)]^2 &= \kappa_t^2 Z_t^2 = \kappa_t^2 \left(\sum_{s=1}^{r_l} \tau_s \cdot (u_s \circ v_s) \right)^2 \\ &= \underbrace{\sum_{s=1}^{r_l} \kappa_t^2 \tau_s^2 \cdot (u_s^2 \circ v_s^2)}_{\text{Separable Term}} + \underbrace{\kappa_t^2 \sum_{p \neq q} \tau_p \tau_q \cdot (u_p u_q \circ v_p v_q)}_{\mathbb{E}_{\tau, u, v} [\tau_p \tau_q \cdot (u_p u_q \circ v_p v_q)] = 0}. \end{aligned} \quad (8)$$

In the above equation, the second term, i.e., the cross term, has an overall expectation of zero on each coordinate. In practice, we test specific cases with different sizes of u_s, v_s and selections of r_l in our experiments. Compared with the first separable term, the impact of the second term becomes negligible. Therefore, our lightweight TeZO-Adam only accumulates the second-order momentum via the first term, i.e. the separable term. This allows us to calculate it via accumulation of the temporal factor vector, similar to how we compute first-order momentum. We first update the $\kappa_t^2 \tau^2$ term and then expand it into the second-order momentum with u_s^2 and v_s^2 . By this way, we only need to store the τ_V vector additionally during training, without being affected by the model dimension d . Due to page limitation, we provide more studies on the precision and efficiency about TeZO-Adam in Appendix A.2.

Advantages of TeZO. Existing works mainly consider the low-rank efficiency of the ZO-SGD method, while the extensions to other optimizers remain inefficient. TeZO not only takes into account the properties of a joint low-rankness, but also serves as an extension-friendly ZO design. It maintains both high memory and computational efficiency across several classical optimizers. This also brings significant benefits for fine-tuning LLMs in practice.

5. Theoretical Analysis

In this section, we mainly introduce the theoretical analysis of TeZO, including fundamental properties and convergence guarantees in the application of various optimizers. Due to space limitation, all proofs are detailed in the Appendix B.

Theorem 1 (Expectation and Variance). *Without loss of generality, we consider the 2D parameters $W \in \mathbb{R}^{m \times n}$. Its*

FO gradient is denoted as $\nabla_W f$ and ZO gradient is denoted as $\nabla_W^0 f$. When using the TeZO method to estimate the ZO gradient with rank r and a sufficiently small perturbation rate ρ as shown in Algorithm 1, the following holds:

$$\begin{aligned} \mathbb{E}_{\tau, u, v} \left[\frac{1}{r} \lim_{\rho \rightarrow 0} \nabla_W^0 f \right] &= \nabla_W f, \\ \mathbb{E}_{\tau, u, v} \left\| \frac{1}{r} \lim_{\rho \rightarrow 0} \nabla_W^0 f - \nabla_W f \right\|^2 &= \delta \|\nabla_W f\|^2, \end{aligned} \quad (9)$$

where $\delta = 1 + mn + \frac{2mn}{r} + \frac{6(m+n)}{r} + \frac{10}{r}$.

Remark 1. TeZO is an unbiased zero-order estimator and its variance is linearly correlated with the norm of the FO gradient. Moreover, we provide detailed relationships between the variance coefficient δ_l and the matrix sizes m_l, n_l as well as rank r_l . Previous work (Yu et al., 2024) focuses on the impact of low-rankness on variance from the perspective of the subspace for the quadratic objective. We provide the formal expression under the low-rank representation for a general smooth objective. The variance for low-rank representation is slightly larger than that of the MeZO method, i.e. mn , remaining within the same order. This indicates that TeZO has comparable ability to MeZO in practice while requiring significantly less training costs.

Then we consider the convergence. In this paper, we consider the general smooth and non-convex function under:

Assumption 1. $f(\cdot)$ is a smooth and nonconvex objective, i.e., for $\forall x, y \in \mathbb{R}^d$, $\|\nabla f(x, \xi) - \nabla f(y, \xi)\| \leq \lambda \|x - y\|$.

Assumption 2. The stochastic gradient is an unbiased estimator with bounded variance, i.e., for each data sample ξ , $\mathbb{E}_\xi [\nabla f(x, \xi)] = \nabla f(x)$, $\mathbb{E}_\xi \|\nabla f(x, \xi) - \nabla f(x)\|^2 \leq \sigma^2$.

These are two commonly adopted assumptions in ZO optimization. Prior works (Chen et al., 2024; Yu et al., 2024) consistently impose the requirement that some or all factor vectors exhibit column orthogonality. In contrast, our proof does not rely on the need for such additional constraints.

Theorem 2 (Convergence). *Without loss of generality, we consider the 2D parameters $W \in \mathbb{R}^{m \times n}$. Under Assumption 1 and 2, let $\eta = \mathcal{O} \left(\sqrt{\frac{D_0}{\lambda T (\rho^2 \lambda^2 \delta_\rho + \delta \sigma^2)}} \right) \leq \frac{1}{\lambda(\delta+1)}$ where $D_0 = f(W_0) - f(W_*)$ is the initialized bias, the sequence $\{W_t\}_{t=0}^{T-1}$ generated by TeZO converges as:*

$$\frac{1}{T} \sum_{t=0}^{T-1} \mathbb{E} \|\nabla f(W_t)\|^2 = \mathcal{O} \left(\sqrt{\frac{\lambda D_0 (\rho^2 \lambda^2 \delta_\rho + \delta \sigma^2)}{T}} \right), \quad (10)$$

where $\delta_\rho = \frac{15r^2(m+3)^3(n+3)^3 + 36r^3m^3n^3 + r^4m^3n^3}{4}$ and δ is defined in Theorem 1.

Remark 2. This convergence result maintains the same rate of recent ZO advances. By substituting the total parameters for d , we have $\delta = \mathcal{O}(d)$ and $\delta_\rho = \mathcal{O}(d^3)$. Let the

Table 3. Experiments of fine-tuning for 80k iterations on RoBERTa-large and then perform evaluations. FT: FO fine-tuning (5 epochs with Adam). ZERO-SHOT: test only. **AVG.** measures the average gap across all datasets compared to FT (+0).

	$k = 16$						$k = 512$					
	SST-5	SNLI	MNLI	QNLI	TREC	AVG.	SST-5	SNLI	MNLI	QNLI	TREC	AVG.
FT	45.0	71.9	65.3	70.6	87.4	+0	57.5	88.3	84.2	87.5	97.2	+0
ZERO-SHOT	22.0	33.7	34.0	52.6	20.4	-35.5	22.0	33.7	34.0	52.6	20.4	-50.4
MEZO	44.7	67.6	60.9	64.8	58.6	-8.7	56.4	83.2	79.5	83.3	95.6	-3.3
SUBZO	44.8	65.7	62.8	64.7	56.6	-9.1	55.7	83.1	80.1	83.7	95.4	-3.3
LOZO	42.0	67.1	60.2	64.7	61.2	-9.0	56.0	84.0	81.6	82.4	95.4	-3.1
TEZO	42.8	67.6	61.8	64.1	57.4	-9.3	54.7	84.0	79.3	82.7	95.8	-3.6
MEZO-M	44.5	67.6	62.1	65.9	61.1	-7.8	56.6	83.4	79.9	83.4	95.4	-3.2
LOZO-M	44.1	67.8	61.3	64.2	62.2	-8.1	55.6	84.1	80.1	82.4	94.6	-3.6
TEZO-M	43.8	67.0	61.1	65.0	60.4	-8.5	54.5	84.4	79.9	82.9	95.5	-3.4

Table 4. Experiments of fine-tuning for 15k iterations on OPT-13B. Other setups are consistent with the Table 3.

	SST-2	RTE	CB	BoolQ	WSC	WIC	MultiRC	COPA	ReCoRD	SQuAD	DROP	AVG.
FT	91.5	70.7	84.0	76.4	63.5	70.0	71.1	79.0	74.1	84.7	31.5	+0
ZERO-SHOT	58.5	59.4	46.4	59.1	38.3	55.2	46.7	80.0	81.0	46.6	14.4	-19.2
MEZO	90.1	60.3	67.9	66.1	62.5	54.7	57.7	87.0	81.1	79.6	30.4	-5.4
SUBZO	91.3	61.9	67.9	66.1	63.5	55.9	57.3	86.0	81.9	80.7	30.5	-4.8
LOZO	90.3	62.5	67.9	65.6	63.5	55.3	56.9	86.0	81.8	80.5	30.1	-5.1
TEZO	90.2	61.1	69.6	65.1	63.5	54.3	56.8	87.0	81.2	80.7	29.6	-5.2
MEZO-M	90.6	60.7	67.9	65.5	62.5	54.6	57.9	88.0	81.5	79.5	30.4	-5.2
LOZO-M	90.7	62.1	67.1	65.7	62.5	55.7	57.7	88.0	81.7	80.7	29.8	-4.9
TEZO-M	91.1	61.4	69.6	64.6	63.5	55.6	56.7	88.0	81.3	80.9	30.0	-4.8
MEZO-ADAM	92.4	70.5	67.9	70.0	62.5	58.7	58.9	88.0	81.1	80.8	30.5	-3.2
ZO-ADAMU	92.0	72.9	67.9	71.0	61.5	59.7	58.4	86.0	81.5	82.4	31.1	-2.9
TEZO-ADAM	93.3	71.8	69.6	71.8	59.9	60.5	60.3	86.0	81.5	84.0	29.8	-2.5

perturbation rate $\rho = \mathcal{O}(\frac{\sigma}{\lambda}d^{-1})$, we have the final rate as $\mathcal{O}(\sqrt{\frac{\lambda D_0 d \sigma^2}{T}})$ which recovers the general rate of the recent ZO methods. This also demonstrates the advantages of the TeZO method, as it reduces the complexity of random sample generation from $\mathcal{O}(d \cdot T)$ to $\mathcal{O}(\sqrt{d} \cdot T)$ and effectively decreases memory usage, while theoretically maintaining the similar convergence rate.

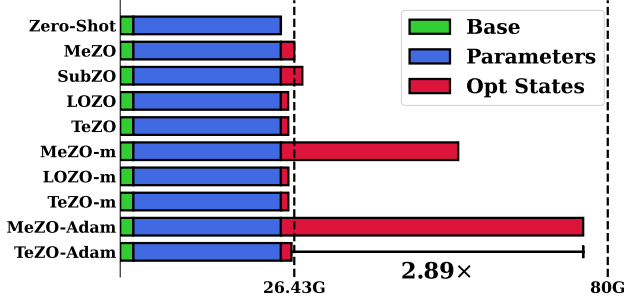
6. Experiments

In this section, we mainly show the empirical studies. We follow the recent studies of fine-tuning LLMs tasks with ZO methods (Malladi et al., 2023; Yu et al., 2024; Chen et al., 2024; Jiang et al., 2024) and adopt the similar setups to validate the efficiency. The main text primarily introduces baselines, performance evaluations, and training costs. Due to page limitations, other contents, including experimental details, hyperparameter selections and some interesting validation results, have been placed in Appendix A.

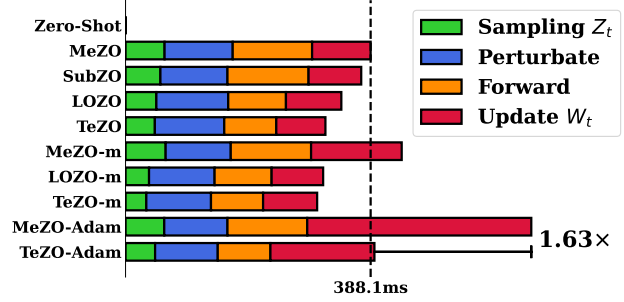
Baselines and setups. We select recent advances of ZO and low-rank ZO methods on fine-tuning LLM tasks as base-

lines, including MeZO (Malladi et al., 2023), LOZO (Chen et al., 2024), SubZO (Yu et al., 2024), and their variants of momentum-based and Adam-based extensions in their works. We also compare ZO-AdaMU (Jiang et al., 2024) which focuses on adaptivity. Similar to these works, we conducted tests on different models, including RoBERTa-large (Liu et al., 1907), OPT (Zhang et al., 2022), and LLaMA (Touvron et al., 2023). We select a total of 16 datasets for testing and compute the final average performance to fairly compare the overall efficiency of each method.

Medium-sized Models. We conduct the experiments on the RoBERTa-large model for the general sentiment classification, natural language inference and text retrieval tasks, as shown in Table 3. To eliminate experimental randomness, the reported results are the averages of 5 runs with different random seeds. It clearly demonstrates the efficiency of the ZO method on medium-sized models. In fact, for medium-sized models, MeZO remains the most accurate ZO method. However, the gap between other low-rank methods and MeZO is not significant, not exceeding 0.6% at the worst scenario on average. In the environment with $k = 512$, almost all ZO methods show no significant differences.



(a) GPU Memory usage on fine-tuning OPT-13B.



(b) Wall-clock time / iteration on fine-tuning OPT-13B.

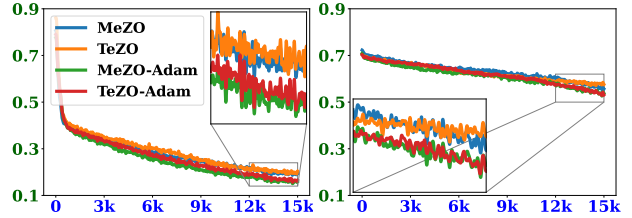
Figure 3. GPU memory usage (a) and wall-clock time (b) for fine-tuning LLMs with RTE dataset on H100. SubZO does not provide other memory-efficient extensions. LOZO does not provide the memory-efficient Adam extension. More details are stated in Appendix A.4.

Table 5. Experiments of fine-tuning 15k iterations on LLaMA-7B. Other setups are consistent with the Table 3.

	SST-2	RTE	WSC	WIC	AVG.
FT	95.6	86.3	64.4	70.4	+0
ZERO-SHOT	59.7	49.8	56.7	50.6	-25.0
MEZO	93.7	69.0	56.6	60.5	-9.2
SUBZO	93.1	67.9	59.7	59.3	-9.2
LOZO	93.6	69.5	59.6	60.2	-8.4
TEZO	92.9	67.0	59.7	59.9	-9.2
MEZO-ADAM	94.4	71.4	58.9	61.9	-7.5
TEZO-ADAM	94.2	75.0	58.9	60.8	-7.0

Large-sized Models. We conduct experiments on LLaMA-7B and OPT-13B, as shown in Table 4, 5. Similarly, the reported results are the averages of 2 runs with different random seeds. On the large models, the low-rank ZO methods generally perform better than MeZO on OPT-13B and maintain similar performance on LLaMA-7B. The variants based on momentum and Adam perform better. MeZO-m and MeZO-Adam can achieve about 0.2% and 2.1% improvements. Due to the strong low-rank nature of TeZO, the alignment of factor vectors used in adaptivity still retains strong subspace properties. In practical training, the benefit of this advantage is that it constantly enforces the adaptive learning rate to stay synchronized with the structured subspace. Therefore, TeZO-Adam can achieve the better performance, about 2.2% improvement on LLaMA-7B and 2.8% improvement on OPT-13B compared to MeZO.

Memory Usage and Wall-clock Time. We evaluate the practical GPU memory usage and wall-clock time for different methods. Figure 3. (a) shows the memory cost of ZO mainly consists of two parts, parameters and optimizer states. For the MeZO baseline, -Adam variant typically consumes 3 \times the storage. However, our proposed TeZO-Adam method requires less storage than MeZO, and is significantly lower than MeZO-Adam ($\sim 34.6\%$). Figure 3. (b) shows the wall-clock time comparisons, primarily including sampling,



(a) Training loss on SST-2. (b) Training loss on RTE.

Figure 4. Loss curves of LLaMA-7B on SST-2 and RTE datasets on ZO-SGD and ZO-Adam methods. We use gaussian_filter1d function in the scipy.ndimage lib to smooth curves with sigma=30.

perturbations, forward pass, and update parameters. our TeZO-Adam maintains a speed comparable to the MeZO and is 1.63 \times faster than MeZO-Adam on one H100 device.

Better Performance in Adaptive ZO. Figure 4. illustrates the significant performance of adaptive ZO methods. It can be observed that the training loss curves of the ZO-SGD methods are nearly identical, indicating that these methods exhibit comparable performance. In contrast, the ZO-Adam method demonstrates superior performance, with a more pronounced reduction in loss curves and more thorough convergence during training, yielding better performance.

7. Conclusion

Inspired by the similarity in the gradient subspace, in this paper, we combine the low-rank properties in both the model and the temporal dimension and propose a novel low-rank ZO method, named TeZO. Moreover, TeZO can easily implement memory-efficient variants of momentum and Adam, maintaining the same resource consumption as standard ZO-SGD, but with better performance. We prove that TeZO maintains the same convergence rate as previous low-rank ZO methods while requiring fewer training costs. Furthermore, we conduct extensive evaluations of TeZO and its variants in fine-tuning tasks of LLMs, which demonstrates the significant potential of low-rank ZO methods.

References

- Achiam, J., Adler, S., Agarwal, S., Ahmad, L., Akkaya, I., Aleman, F. L., Almeida, D., Altenschmidt, J., Altman, S., Anadkat, S., et al. Gpt-4 technical report. *arXiv preprint arXiv:2303.08774*, 2023.
- Brown, T., Mann, B., Ryder, N., Subbiah, M., Kaplan, J. D., Dhariwal, P., Neelakantan, A., Shyam, P., Sastry, G., Askell, A., et al. Language models are few-shot learners. *Advances in neural information processing systems*, 33: 1877–1901, 2020.
- Chen, A., Zhang, Y., Jia, J., Diffenderfer, J., Liu, J., Parasyris, K., Zhang, Y., Zhang, Z., Kailkhura, B., and Liu, S. Deepzero: Scaling up zeroth-order optimization for deep model training. *arXiv preprint arXiv:2310.02025*, 2023.
- Chen, P.-Y., Zhang, H., Sharma, Y., Yi, J., and Hsieh, C.-J. Zoo: Zeroth order optimization based black-box attacks to deep neural networks without training substitute models. In *Proceedings of the 10th ACM workshop on artificial intelligence and security*, pp. 15–26, 2017.
- Chen, Y., Zhang, Y., Cao, L., Yuan, K., and Wen, Z. Enhancing zeroth-order fine-tuning for language models with low-rank structures. *arXiv preprint arXiv:2410.07698*, 2024.
- Cheng, S., Wu, G., and Zhu, J. On the convergence of prior-guided zeroth-order optimization algorithms. *Advances in Neural Information Processing Systems*, 34:14620–14631, 2021.
- Fang, W., Yu, Z., Jiang, Y., Shi, Y., Jones, C. N., and Zhou, Y. Communication-efficient stochastic zeroth-order optimization for federated learning. *IEEE Transactions on Signal Processing*, 70:5058–5073, 2022.
- Gautam, T., Park, Y., Zhou, H., Raman, P., and Ha, W. Variance-reduced zeroth-order methods for fine-tuning language models. *arXiv preprint arXiv:2404.08080*, 2024.
- Ghadimi, S. and Lan, G. Stochastic first-and zeroth-order methods for nonconvex stochastic programming. *SIAM journal on optimization*, 23(4):2341–2368, 2013.
- Golovin, D., Karro, J., Kochanski, G., Lee, C., Song, X., and Zhang, Q. Gradientless descent: High-dimensional zeroth-order optimization. *arXiv preprint arXiv:1911.06317*, 2019.
- Gratton, C., Venkategowda, N. K., Arablouei, R., and Werner, S. Privacy-preserved distributed learning with zeroth-order optimization. *IEEE Transactions on Information Forensics and Security*, 17:265–279, 2021.
- Guo, W., Long, J., Zeng, Y., Liu, Z., Yang, X., Ran, Y., Gardner, J. R., Bastani, O., De Sa, C., Yu, X., et al. Zeroth-order fine-tuning of llms with extreme sparsity. *arXiv preprint arXiv:2406.02913*, 2024.
- Gupta, D., Razaviyayn, M., and Sharan, V. On the inherent privacy of two point zeroth order projected gradient descent. In *OPT 2024: Optimization for Machine Learning*.
- Hajinezhad, D., Hong, M., and Garcia, A. Zone: Zeroth-order nonconvex multiagent optimization over networks. *IEEE transactions on automatic control*, 64(10):3995–4010, 2019.
- Hitchcock, F. L. The expression of a tensor or a polyadic as a sum of products. *Journal of Mathematics and Physics*, 6(1-4):164–189, 1927.
- Hu, E. J., Shen, Y., Wallis, P., Allen-Zhu, Z., Li, Y., Wang, S., Wang, L., and Chen, W. Lora: Low-rank adaptation of large language models. *arXiv preprint arXiv:2106.09685*, 2021.
- Huang, F., Gao, S., Pei, J., and Huang, H. Nonconvex zeroth-order stochastic admm methods with lower function query complexity. *IEEE Transactions on Pattern Analysis and Machine Intelligence*, 2024.
- Jaiswal, A., Yin, L., Zhang, Z., Liu, S., Zhao, J., Tian, Y., and Wang, Z. From galore to welore: How low-rank weights non-uniformly emerge from low-rank gradients. *arXiv preprint arXiv:2407.11239*, 2024.
- Ji, K., Wang, Z., Zhou, Y., and Liang, Y. Improved zeroth-order variance reduced algorithms and analysis for non-convex optimization. In *International conference on machine learning*, pp. 3100–3109. PMLR, 2019.
- Jiang, S., Chen, Q., Pan, Y., Xiang, Y., Lin, Y., Wu, X., Liu, C., and Song, X. Zo-adamu optimizer: Adapting perturbation by the momentum and uncertainty in zeroth-order optimization. In *Proceedings of the AAAI Conference on Artificial Intelligence*, volume 38, pp. 18363–18371, 2024.
- Kariyappa, S., Prakash, A., and Qureshi, M. K. Maze: Data-free model stealing attack using zeroth-order gradient estimation. In *Proceedings of the IEEE/CVF Conference on Computer Vision and Pattern Recognition*, pp. 13814–13823, 2021.
- Kazemi, E. and Wang, L. Efficient zeroth-order proximal stochastic method for nonconvex nonsmooth black-box problems. *Machine Learning*, 113(1):97–120, 2024.
- Kojima, T., Gu, S. S., Reid, M., Matsuo, Y., and Iwasawa, Y. Large language models are zero-shot reasoners. *Advances in neural information processing systems*, 35: 22199–22213, 2022.

- Liu, S., Chen, J., Chen, P.-Y., and Hero, A. Zeroth-order on-line alternating direction method of multipliers: Convergence analysis and applications. In *International Conference on Artificial Intelligence and Statistics*, pp. 288–297. PMLR, 2018a.
- Liu, S., Kailkhura, B., Chen, P.-Y., Ting, P., Chang, S., and Amini, L. Zeroth-order stochastic variance reduction for nonconvex optimization. *Advances in Neural Information Processing Systems*, 31, 2018b.
- Liu, S., Chen, P.-Y., Kailkhura, B., Zhang, G., Hero III, A. O., and Varshney, P. K. A primer on zeroth-order optimization in signal processing and machine learning: Principals, recent advances, and applications. *IEEE Signal Processing Magazine*, 37(5):43–54, 2020.
- Liu, Y., Ott, M., Goyal, N., Du, J., Joshi, M., Chen, D., Levy, O., Lewis, M., Zettlemoyer, L., and Stoyanov, V. Roberta: A robustly optimized bert pretraining approach. arxiv [preprint](2019). *arXiv preprint arXiv:1907.11692*, 1907.
- Liu, Y., Zhu, Z., Gong, C., Cheng, M., Hsieh, C.-J., and You, Y. Sparse mezo: Less parameters for better performance in zeroth-order llm fine-tuning. *arXiv preprint arXiv:2402.15751*, 2024.
- Malladi, S., Gao, T., Nichani, E., Damian, A., Lee, J. D., Chen, D., and Arora, S. Fine-tuning language models with just forward passes. *Advances in Neural Information Processing Systems*, 36:53038–53075, 2023.
- Maritan, A. and Schenato, L. Zo-jade: Zeroth-order curvature-aware distributed multi-agent convex optimization. *IEEE Control Systems Letters*, 7:1813–1818, 2023.
- Mukhoty, B., Bojkovic, V., de Vazelhes, W., Zhao, X., De Masi, G., Xiong, H., and Gu, B. Direct training of snn using local zeroth order method. *Advances in Neural Information Processing Systems*, 36:18994–19014, 2023.
- Naveed, H., Khan, A. U., Qiu, S., Saqib, M., Anwar, S., Usman, M., Akhtar, N., Barnes, N., and Mian, A. A comprehensive overview of large language models. *arXiv preprint arXiv:2307.06435*, 2023.
- Nesterov, Y. and Spokoiny, V. Random gradient-free minimization of convex functions. *Foundations of Computational Mathematics*, 17(2):527–566, 2017.
- Nikolakakis, K., Haddadpour, F., Kalogerias, D., and Karbasi, A. Black-box generalization: Stability of zeroth-order learning. *Advances in neural information processing systems*, 35:31525–31541, 2022.
- Rando, M., Molinari, C., Rosasco, L., and Villa, S. An optimal structured zeroth-order algorithm for non-smooth optimization. *Advances in Neural Information Processing Systems*, 36, 2024.
- Shen, L., Sun, Y., Yu, Z., Ding, L., Tian, X., and Tao, D. On efficient training of large-scale deep learning models: A literature review. *arXiv preprint arXiv:2304.03589*, 2023.
- Spall, J. C. Multivariate stochastic approximation using a simultaneous perturbation gradient approximation. *IEEE transactions on automatic control*, 37(3):332–341, 1992.
- Tang, Y., Zhang, J., and Li, N. Distributed zero-order algorithms for nonconvex multiagent optimization. *IEEE Transactions on Control of Network Systems*, 8(1):269–281, 2020.
- Touvron, H., Lavril, T., Izacard, G., Martinet, X., Lachaux, M.-A., Lacroix, T., Rozière, B., Goyal, N., Hambro, E., Azhar, F., et al. Llama: Open and efficient foundation language models. *arXiv preprint arXiv:2302.13971*, 2023.
- Tu, C.-C., Ting, P., Chen, P.-Y., Liu, S., Zhang, H., Yi, J., Hsieh, C.-J., and Cheng, S.-M. Autozoom: Autoencoder-based zeroth order optimization method for attacking black-box neural networks. In *Proceedings of the AAAI conference on artificial intelligence*, volume 33, pp. 742–749, 2019.
- Vemula, A., Sun, W., and Bagnell, J. Contrasting exploration in parameter and action space: A zeroth-order optimization perspective. In *The 22nd International Conference on Artificial Intelligence and Statistics*, pp. 2926–2935. PMLR, 2019.
- Wang, F., Shen, L., Ding, L., Xue, C., Liu, Y., and Ding, C. Simultaneous computation and memory efficient zeroth-order optimizer for fine-tuning large language models. *arXiv preprint arXiv:2410.09823*, 2024a.
- Wang, H., Agarwal, S., Tanaka, Y., Xing, E., Papailiopoulos, D., et al. Cuttlefish: Low-rank model training without all the tuning. *Proceedings of Machine Learning and Systems*, 5:578–605, 2023.
- Wang, Y., Du, S., Balakrishnan, S., and Singh, A. Stochastic zeroth-order optimization in high dimensions. In *International conference on artificial intelligence and statistics*, pp. 1356–1365. PMLR, 2018.
- Wang, Z., Zhang, M., Yang, J., Shao, B., and Zhang, M. Maft: Efficient model-agnostic fairness testing for deep neural networks via zero-order gradient search. In *Proceedings of the IEEE/ACM 46th International Conference on Software Engineering*, pp. 1–12, 2024b.
- Yang, Y., Zhen, K., Banijamal, E., Mouchtaris, A., and Zhang, Z. Adazeta: Adaptive zeroth-order tensor-train adaption for memory-efficient large language models fine-tuning. *arXiv preprint arXiv:2406.18060*, 2024.

-
- Yi, X., Zhang, S., Yang, T., Chai, T., and Johansson, K. H. Linear convergence of first-and zeroth-order primal–dual algorithms for distributed nonconvex optimization. *IEEE Transactions on Automatic Control*, 67(8):4194–4201, 2021.
- Yu, Z., Zhou, P., Wang, S., Li, J., and Huang, H. Subzero: Random subspace zeroth-order optimization for memory-efficient llm fine-tuning. *arXiv preprint arXiv:2410.08989*, 2024.
- Zhang, L., Thekumparampil, K. K., Oh, S., and He, N. Dpzero: dimension-independent and differentially private zeroth-order optimization. In *International Workshop on Federated Learning in the Age of Foundation Models in Conjunction with NeurIPS 2023*, 2023.
- Zhang, S., Roller, S., Goyal, N., Artetxe, M., Chen, M., Chen, S., Dewan, C., Diab, M., Li, X., Lin, X. V., et al. Opt: Open pre-trained transformer language models. *arXiv preprint arXiv:2205.01068*, 2022.
- Zhao, H., Li, J., Pan, Y., Liang, S., Yang, X., Liu, W., Li, X., Dou, F., Liu, T., and Lu, J. Helene: Hessian layer-wise clipping and gradient annealing for accelerating fine-tuning llm with zeroth-order optimization. *arXiv preprint arXiv:2411.10696*, 2024a.
- Zhao, J., Zhang, Z., Chen, B., Wang, Z., Anandkumar, A., and Tian, Y. Galore: Memory-efficient llm training by gradient low-rank projection. *arXiv preprint arXiv:2403.03507*, 2024b.
- Zhao, P., Chen, P.-Y., Wang, S., and Lin, X. Towards query-efficient black-box adversary with zeroth-order natural gradient descent. In *Proceedings of the AAAI Conference on Artificial Intelligence*, volume 34, pp. 6909–6916, 2020.
- Zhao, W. X., Zhou, K., Li, J., Tang, T., Wang, X., Hou, Y., Min, Y., Zhang, B., Zhang, J., Dong, Z., et al. A survey of large language models. *arXiv preprint arXiv:2303.18223*, 2023.
- Zhao, Y., Dang, S., Ye, H., Dai, G., Qian, Y., and Tsang, I. W. Second-order fine-tuning without pain for llms: A hessian informed zeroth-order optimizer. *arXiv preprint arXiv:2402.15173*, 2024c.

A. Experiment Materials

A.1. Low Rankness in LLMs

This property has been well studied and validated by several works. Especially in large models, the low-rank nature of parameters, gradients, and the FO optimizer states have triggered a series of studies. The most representative works include LoRA low-rank structure (Hu et al., 2021), GaLore low-rank optimization (Zhao et al., 2024b), and so on. In the main text, we study the low-rankness on the OPT-1.3B model. Here, we also show tests of the low-rankness on the LLaMA-7B.

A.1.1. LOW RANKNESS OF EACH SINGLE GRADIENT

We first learn the low rankness of each single gradient. Similarly, we consider the 2D parameters $W_l \in \mathbb{R}^{m \times n}$. Then we calculate the top-100 singular values of its gradients $\nabla_{W_l} f \in \mathbb{R}^{m \times n}$ to test the low-rankness, As shown in Figure 5.

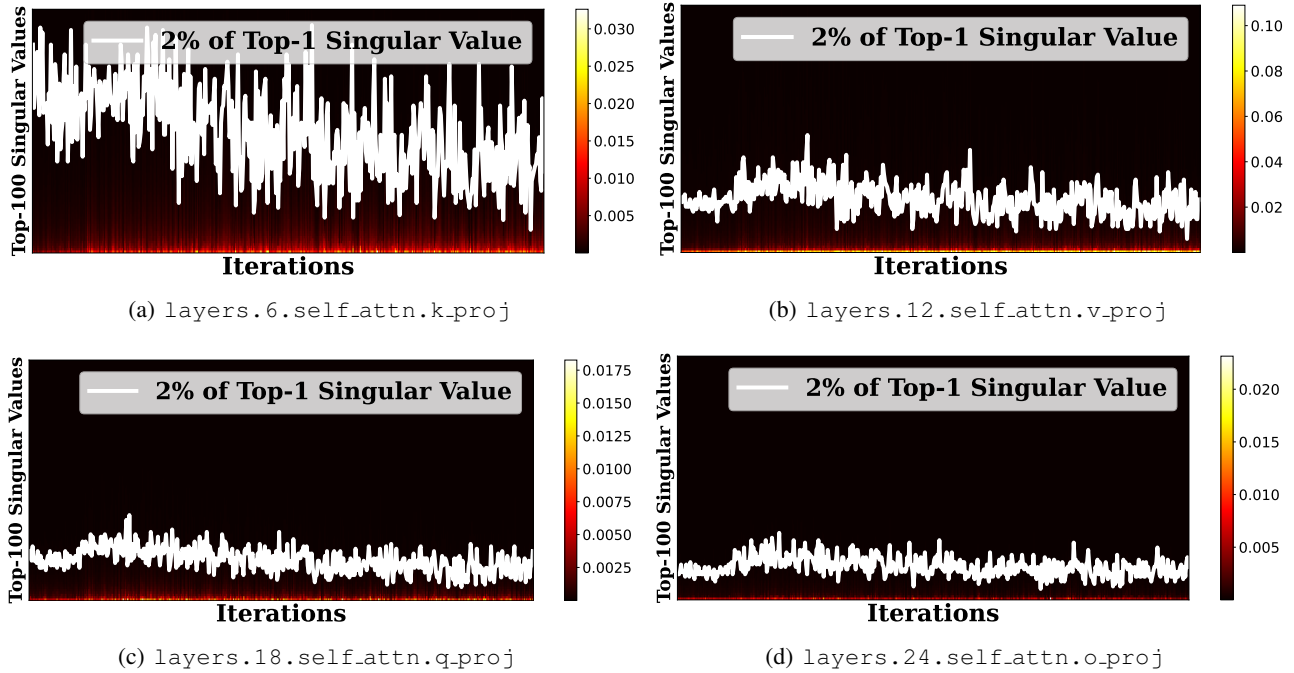


Figure 5. We finetune LLaMA-7B on SST-2 to test low-rankness of gradients. We set the batchsize as 16 and train 500 steps with 8000 samples on a H200 device. The training loss decreases from 1.04 to 0.13. We analyze the low-rank properties of the W_K , W_V , W_Q and W_O parameters in the 6-th, 12-th, 18-th, and 24-th modules at each iteration ($W_K, W_V, W_Q, W_O \in \mathbb{R}^{4096 \times 4096}$). The white lines represent the indices where the singular values are 2% of the maximum singular value.

It is clear that gradients are low-rank on LLaMA-7B model and the low-rankness is even greater than that of OPT-1.3B. After around index-20, the singular value is almost completely lost. It is worth noting that in our tests, **the data samples used for each gradient computation are completely different**, which further emphasizes the universality of gradient low-rankness in LLMs.

A.1.2. LOW RANKNESS OF GRADIENT SUBSPACE

The low-rankness of each individual gradient has already been widely acknowledged. In this part, we continue to explore the low-rank subspace of all gradients in the LLaMA-7B model. The same, we consider the 2D parameters $W_l \in \mathbb{R}^{m \times n}$ trained for T iterations. We normalize each flattened gradient and concatenate them along the T dimension to form a new matrix as $G = [g_{w_l,0}, g_{w_l,1}, \dots, g_{w_l,T}] \in \mathbb{R}^{mn \times T}$ where $g_{w_l,t} = \nabla_{w_l} f_t / \|\nabla_{w_l} f_t\| \in \mathbb{R}^{mn}$. And then we calculate the cosine value by $G^\top G$. It is important to note that **without normalization, the low-rankness of this matrix naturally holds**. This is because when the loss is large, the gradients are naturally large. As training progresses and the loss becomes smaller, the gradients will be much smaller. If these gradients are concatenated directly, although it still forms a low-rank matrix, this

low-rank nature is inconsistent with the motivation behind our proposed TeZO method. TeZO expects similarity across the entire gradient space. Since we are always more concerned with whether the gradient direction is similar, we study the properties of each normalized gradient, specifically whether all gradients lie in the same subspace, as shown in *Figure 6*.

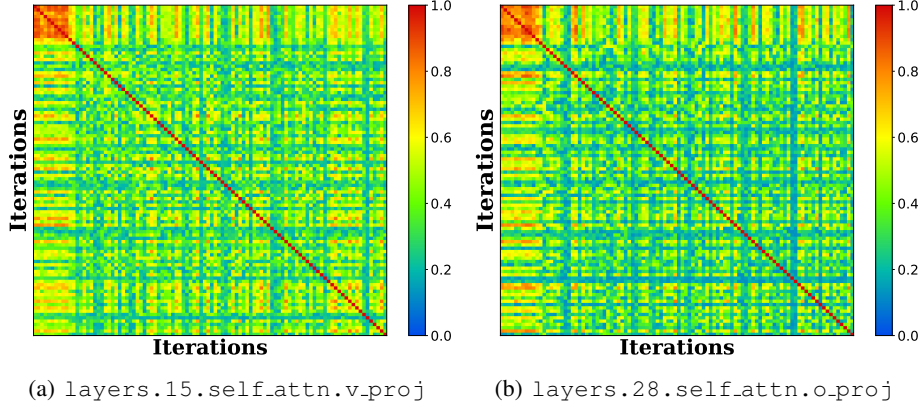


Figure 6. We finetune LLaMA-7B on SST-2 to test the similarity between gradients at different iterations. Similarly, we set the batchsize as 16 and train 500 steps with 8000 samples on a H200 device. The training loss decreases from 1.04 to 0.13. We calculate the cosine value of each gradient pair ($\nabla_{W_i} f_{t_1}, \nabla_{W_i} f_{t_2}$) where $t_1, t_2 \in [0, 1, 2, \dots, 499]$ and show their values as the heat maps above.

It can be seen that the similarity between gradients is generally high, and the distribution of cosine distances is relatively concentrated. This also highlights the low-rankness of the gradient space in training LLMs, where gradients from different samples exhibit strong similarity.

A.1.3. LOW-RANKNESS BETWEEN WEIGHTS AND GRADIENTS

In this part, we explore the close relationship between the low-rankness of gradients and that of model parameters.

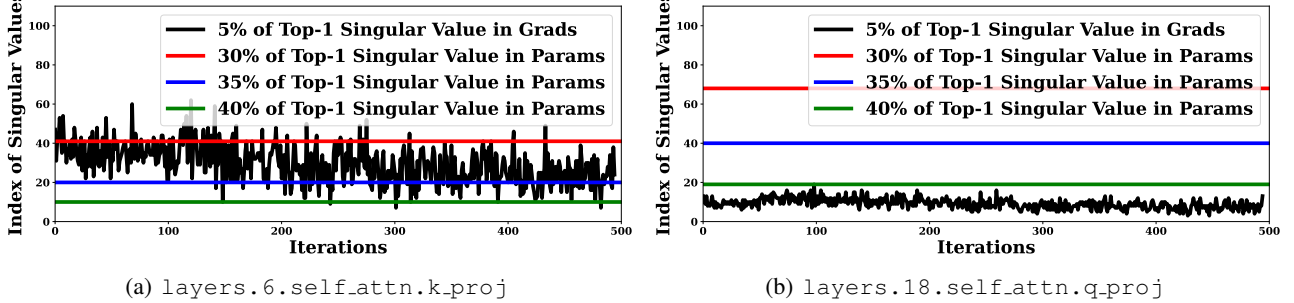


Figure 7. We finetune LLaMA-7B on SST-2 to test the similarity between gradients at different iterations. We compared the relationship between the low-rank properties of parameters and gradients, and demonstrat the rank levels of parameters.

We can observe that, although the degree of low-rankness in gradients and parameters is not strictly aligned, they still exhibit a high degree of correlation within a certain fluctuation range. In fact, due to the very small learning rate, the gradient updates for individual parameters are negligible, which allows the low-rank nature of the model to remain relatively stable. This also validates the effectiveness of our dynamic selection method within a certain range. The dynamic selection method eliminates the need for additional hyperparameter tuning while ensuring experimental stability.

A.2. The Efficiency of Lightweight Second-order Momentum in TeZO-Adam

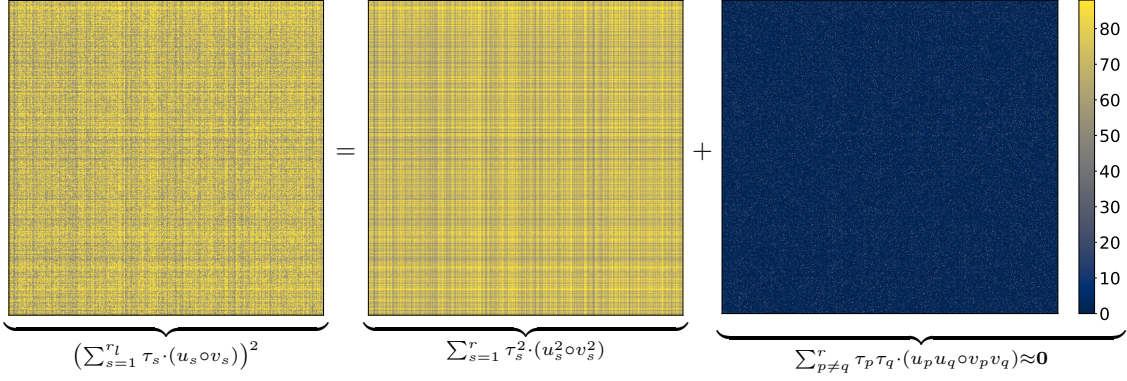
In this paper, we propose a lightweight variant to address the storage issue of second-order momentum in the TeZO-Adam variant:

$$[\nabla^0 f(w_t)]^2 = \kappa_t^2 Z_t^2 = \kappa_t^2 \left(\sum_{s=1}^{r_l} \tau_s \cdot (u_s \circ v_s) \right)^2 = \underbrace{\sum_{s=1}^{r_l} \kappa_t^2 \tau_s^2 \cdot (u_s^2 \circ v_s^2)}_{\text{Separable Term}} + \underbrace{\kappa_t^2 \sum_{p \neq q}^{r_l} \tau_p \tau_q \cdot (u_p u_q \circ v_p v_q)}_{\mathbb{E}_{\tau, u, v} [\tau_p \tau_q \cdot (u_p u_q \circ v_p v_q)] = 0}. \quad (11)$$

The separable term is memory-efficient which can be calculated by the accumulation of the factor vector τ .

A.2.1. ERRORS IN ONE STEP

By the definitions, we consider the decomposition of $Z \in \mathbb{R}^{m \times n}$ by the factor vectors $u_s \in \mathbb{R}^m$, $v_s \in \mathbb{R}^n$, and $\tau \in \mathbb{R}^r$. And we consider an example comparable in scale to the LLaMA-7B model and set $m = n = 4096$. And we select $r = 64$ to evaluate the error. Since we consider the parameters at time t where κ_t can be treated as a constant. Without loss of generality, we set $\kappa_t = 1$ directly and examine the error by randomly sampling τ, u, v , as shown in the following figure.



This clearly demonstrates the precision of our lightweight estimation. The second term is almost zero, and the cost of calculating it is very high, including both storage and computation. Therefore, we eliminate the second term directly and accumulate the second-order momentum of the first term as the second-order momentum of Adam for updates. This significantly reduces the training cost, making the training overhead of our TeZO-Adam method almost consistent with that of MeZO-SGD, significantly lower than the MeZO-Adam method.

A.2.2. ACCUMULATED ERRORS AFTER T STEPS

Then we learn the accumulated errors in the training process. We define the update of standard second-order momentum as $V_{t+1} = \beta_2 V_t + (1 - \beta_2) (\sum_{s=1}^r \tau_{s,t} \cdot (u_s \circ v_s))^2$, and that of TeZO-Adam as $\hat{V}_{t+1} = \beta_2 \hat{V}_t + (1 - \beta_2) \sum_{s=1}^r \tau_{s,t}^2 \cdot (u_s^2 \circ v_s^2)$. We report the averaged accumulated errors $E_t = (V_t - \hat{V}_t)/mn$ over 1000 steps under $\beta_2 = 0.99$, as shown in Figure 8.

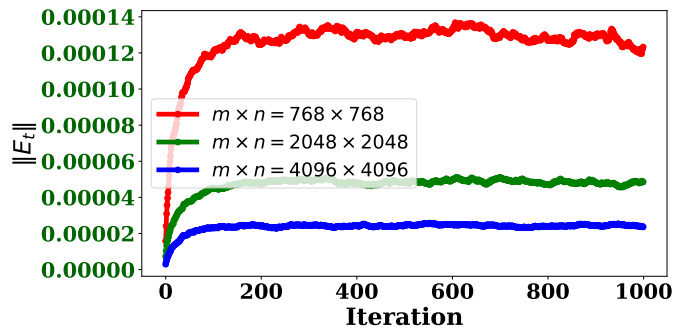


Figure 8. $\|E_t\|$ under different m, n and $r = 64$. It can be observed that the averaged accumulated errors decrease as the model size increases, which highlights the practicality of our proposed lightweight second-order moment estimation on LLMs.

A.3. Setups and Hyperparameters

We follow previous works (Malladi et al., 2023; Chen et al., 2024; Yu et al., 2024) and summarized the range of hyperparameter selections, as shown in Table 6. Although certain hyperparameters, such as batchsize and perturbation rate, may introduce subtle variations, we fix these hyperparameters across all methods to ensure fairness. The primary search hyperparameter is the learning rate across models of different scales.

Table 6. Hyperparameter recommendations for different models.

Method	Hyperparameters	Search Range	RoBERTa-large	OPT-13B	LLaMA-7B
MeZO MeZO-m	Batchsize	{16,32,64}	64	16	
	learning rate	{1e-4, 1e-5, 1e-6, 1e-7}	1e-6	1e-7	1e-6
	perturbation rate	1e-3		1e-3	
MeZO-Adam	Batchsize	{16,32,64}	64	16	
	learning rate	{1e-4, 3e-5, 1e-5, 3e-6}	-	1e-5	3e-5 / 1e-5
	perturbation rate	1e-3		1e-3	
SubZO	Batchsize	{16,32,64}	64	16	
	learning rate	{1e-4, 1e-5, 1e-6, 1e-7}	1e-6	1e-7	1e-6
	perturbation rate	1e-3		1e-3	
	rank	{32, 64, 128}		64	
	lazy update interval	{50, 100, 500}		500	
LOZO LOZO-m	Batchsize	{16,32,64}	64	16	
	learning rate	{1e-4, 1e-5, 1e-6, 1e-7}	1e-6	1e-7	1e-6
	perturbation rate	1e-3		1e-3	
	rank	{8, 16, 32}		8	
	lazy update interval	{50, 100, 500}		100	
TeZO TeZO-m	Batchsize	{16,32,64}	64	16	
	learning rate	{1e-4, 1e-5, 1e-6, 1e-7}	1e-6	1e-7	1e-6
	perturbation rate	1e-3		1e-3	
	threshold to select rank	{20%, 25%, 30%, 35%}		25% / 30%	
	maximum threshold of rank	{32, 64, 128, 256}		depend on tasks	
TeZO-Adam	Batchsize	{16,32,64}	64	16	
	learning rate	{1e-4, 3e-5, 1e-5, 3e-6}	-	1e-5	3e-5 / 1e-5
	perturbation rate	1e-3		1e-3	
	threshold to select rank	{20%, 25%, 30%, 35%}		25% / 30%	
	maximum threshold of rank	{32, 64, 128, 256}		depend on tasks	

We refer to the selections reported in previous works and grid search each hyperparameter. Although further fine-tuning of hyperparameters for specific tasks could yield greater benefits, we fix the hyperparameter selections for fairness. The recommended value reported in the table above is provided only as a reference on which most tasks work well.

A.4. Memory Usage and Wall-clock Time on Different Model Sizes

We extensively test the training efficiency of the OPT and LLaMA models across different model sizes, as shown in *Table 7* and *Table 8*.

Table 7. GPU memory usage (max memory reserved) for fine-tuning LLMs on RTE dataset on a single H100 device.

	OPT						LLaMA		
	125M	1.3B	2.7B	6.7B	13B	30B	7B	13B	30B
Zero-Shot	0.36 G	2.90 G	5.44 G	12.73 G	24.39 G	56.46 G	12.92 G	24.89 G	61.86 G
MeZO	0.57 G	3.48 G	6.40 G	14.40 G	26.43 G	60.31 G	13.91 G	26.12 G	63.77 G
SubZO	0.54 G	3.28 G	5.92 G	14.91 G	26.97 G	61.18 G	14.28 G	26.67 G	64.45 G
LOZO	0.52 G	3.31 G	5.95 G	13.66 G	25.50 G	57.93 G	13.44 G	25.77 G	62.38 G
TeZO	0.54 G	3.28 G	5.92 G	13.68 G	25.52 G	57.95 G	13.47 G	25.79 G	62.40 G
MeZO-m	0.89 G	6.31 G	11.77 G	27.19 G	51.32 G	>80 G	26.85 G	51.31 G	>80 G
LOZO-m	0.53 G	3.32 G	5.97 G	13.68 G	25.53 G	57.99 G	13.47 G	25.80 G	62.44 G
TeZO-m	0.55 G	3.29 G	5.93 G	13.69 G	25.52 G	57.96 G	13.48 G	25.79 G	62.40 G
MeZO-Adam	1.19 G	9.15 G	16.90 G	39.98 G	75.27 G	>80 G	39.50 G	75.69 G	>80 G
TeZO-Adam	0.57 G	3.48 G	6.16 G	14.07 G	26.01 G	58.64 G	13.71 G	26.16 G	62.80 G

Table 8. Wall-clock time per iteration for fine-tuning LLMs on RTE dataset on a single H100 device.

	OPT						LLaMA		
	125M	1.3B	2.7B	6.7B	13B	30B	7B	13B	30B
Zero-Shot	-	-	-	-	-	-	-	-	-
MeZO	33 ms	69 ms	111 ms	212 ms	388 ms	871 ms	212 ms	372 ms	942 ms
SubZO	39 ms	75 ms	121 ms	211 ms	373 ms	939 ms	218 ms	385 ms	988 ms
LOZO	34 ms	71 ms	109 ms	191 ms	341 ms	745 ms	195 ms	350 ms	832 ms
TeZO	36 ms	67 ms	106 ms	178 ms	316 ms	680 ms	186 ms	325 ms	775 ms
MeZO-m	32 ms	76 ms	123 ms	236 ms	437 ms	-	236 ms	422 ms	-
LOZO-m	40 ms	78 ms	104 ms	181 ms	312 ms	677 ms	180 ms	316 ms	759 ms
TeZO-m	37 ms	70 ms	100 ms	172 ms	303 ms	653 ms	176 ms	308 ms	738 ms
MeZO-Adam	39 ms	104 ms	173 ms	348 ms	642 ms	-	342 ms	624 ms	-
TeZO-Adam	54 ms	92 ms	134 ms	224 ms	394 ms	841 ms	227 ms	397 ms	937 ms

From the perspective of memory, low-rank methods have consistently been effective in reducing memory usage. Whether on the OPT or LLaMA models, our TeZO-Adam method consistently incurs lower loss compared to the standard MeZO method, and uses approximately 30% of the memory consumed by the MeZO-Adam method.

From the perspective of wall-clock time, low-rank methods show a significant efficiency improvement on large models, while they perform poorly or even slower on smaller models. On the 125M model, low-rank methods is slower and on the 1.3B models, low-rank methods performs the same as MeZO. Since the model parameters are relatively small, the additional overhead of low-rank computation offsets the training cost. However, when the model size exceeds 3B, the efficiency improvement of low-rank methods becomes significant. Tests on both OPT and LLaMA models show that TeZO-Adam can achieve the same speed as MeZO, while being more than $1.5\times$ faster than MeZO-Adam.

These results are consistent with the *Figure 3* in the main text. From the perspective of computational efficiency, we recommend: **it is better to adopt low-rank ZO methods on models larger than 3B to achieve valid improvements.**

A.5. Low-rank Parameters v.s. Low-rank ZO Methods

Gradient low-rank approximation and model low-rank factorization are two key techniques for efficient training, as we mentioned earlier. Techniques like LoRA (Hu et al., 2021) and GaLore (Zhao et al., 2024b), they reduce the number of trainable model parameters and optimizer states through low-rank mapping and subspace mapping, respectively, thereby accelerating the training process. We want to emphasize that these two methods are orthogonal because they target different parameters, addressing the efficient training of different parts of the models during training. Recent works (Yu et al., 2024; Chen et al., 2024) apply low-rank ZO methods to train LoRA models, achieving some success. Here, we would like to emphasize that, according to the experimental records in Appendix A.4, when the size of trainable parameters is too small, low-rank ZO methods provide almost no benefits. For instance, the LoRA model for the 13B model has approximately 300M parameters, and applying low-rank ZO at this parameter scale is clearly unnecessary. Therefore, in this part, we consider these two techniques as independent methods for comparisons, as shown in Table 9. The other setups are the same as above.

Table 9. GPU memory usage (max memory reserved) for full fine-tuning, fine-tuning LoRA, fine-tuning prefix, and ZO methods.

		OPT-6.7B		OPT-13B	
		Memory	Ratio	Memory	Ratio
FO	ft	105.24 G	8.27×	238.26 G	9.77×
	ft-LoRA	37.96 G	2.98×	73.19 G	3.00×
	ft-prefix	38.23 G	3.00×	73.13 G	3.00×
ZO	MeZO	14.40 G	1.13×	26.43 G	1.08×
	MeZO-LoRA	13.04 G	1.02×	24.82 G	1.02×
	MeZO-prefix	13.06 G	1.03×	24.81 G	1.02×
	MeZO-Adam	39.98 G	3.14×	75.27 G	3.09×
	TeZO-Adam	14.07 G	1.10×	26.01 G	1.06×
	Zero-Shot	12.73 G	1×	24.39 G	1×

Compared to FO methods, the advantages of ZO methods remain significant. Even with methods of low-rank parameters, the memory usage is still nearly three times higher than ZO methods. Additionally, we want to emphasize that while “ZO + LoRA” can further reduce training costs, the gains of memory-efficiency are negligible. Moreover, based on the experiments in existing studies, the performance of these approaches will significantly degrade on large models. “ZO + fine-tuning full parameters” has already achieved to the comparable memory usage of zero-shot (inference only), and combining ZO with LoRA can only save very limited memory. Therefore, we do not advocate directly combining ZO methods with PEFT approaches. From the perspective of memory usage, the benefits of such a combination are indeed limited.

B. Proofs of Main Theorems.

B.1. Proofs of Theorem 1

We consider the mean at first. According to Proposition A.1 proposed by [Chen et al. \(2024\)](#), we have:

$$\lim_{\rho \rightarrow 0} \frac{f(W + \rho Z, \xi) - f(W, \xi) - \langle \nabla f(W, \xi), \rho Z \rangle}{\rho} = 0.$$

Without loss of generality, we consider the case where the parameters are 2D matrix. On each step, we sample $\tau \sim \mathcal{N}(0, I_r)$ and compute the perturbation $Z = \sum_{s=1}^r \tau_s \cdot (u_s \circ v_s)$. By directly expanding the ZO gradient in TeZO , we have:

$$\begin{aligned} \lim_{\rho \rightarrow 0} \nabla^0 f(w, \xi) &= \lim_{\rho \rightarrow 0} \frac{f(W + \rho Z, \xi) - f(W - \rho Z, \xi)}{2\rho} \cdot Z \\ &= \lim_{\rho \rightarrow 0} \frac{f(W + \rho Z, \xi) - f(W, \xi) - \langle \nabla f(W, \xi), \rho Z \rangle}{2\rho} \cdot Z - \lim_{\rho \rightarrow 0} \frac{f(W - \rho Z, \xi) - f(W, \xi) - \langle \nabla f(W, \xi), -\rho Z \rangle}{2\rho} \cdot Z \\ &\quad + \lim_{\rho \rightarrow 0} \frac{\langle \nabla f(W, \xi), \rho Z \rangle}{\rho} \cdot Z = \langle \nabla f(W, \xi), Z \rangle \cdot Z, \end{aligned}$$

where the inner product performs as the calculation in vectors. With Z substituted, the following holds:

$$\lim_{\rho \rightarrow 0} \nabla^0 f(W, \xi) = \left\langle \nabla f(W, \xi), \sum_{s=1}^r \tau_s \cdot (u_s \circ v_s) \right\rangle \cdot \sum_{s=1}^r \tau_s \cdot (u_s \circ v_s).$$

Specifically, we consider the element $[\lim_{\rho \rightarrow 0} \nabla^0 f(w, \xi)]_{i^*, j^*}$. To simplify the expression, we have slightly abused the notation $u_{s,i}$ and $v_{s,j}$, which means the i -th element in vector u_s and j -th element in vector v_s . By taking the expectation,

$$\begin{aligned} \mathbb{E} \left[\lim_{\rho \rightarrow 0} \nabla^0 f(W, \xi) \right]_{i^*, j^*} &= \mathbb{E} \left\langle \nabla f(W, \xi), \sum_{s=1}^r \tau_s \cdot (u_s \circ v_s) \right\rangle \cdot \sum_{s=1}^r \tau_s u_{s,i^*} v_{s,j^*} \\ &= \mathbb{E} \sum_{i,j} \left(\nabla f(W, \xi)_{i,j} \sum_{s=1}^r \tau_s u_{s,i} v_{s,j} \right) \cdot \sum_{s=1}^r \tau_s u_{s,i^*} v_{s,j^*} \\ &= \mathbb{E} \underbrace{\sum_{i \neq i^*, j \neq j^*} \nabla f(W, \xi)_{i,j} \sum_{s,s'}^r \tau_s \tau_{s'} u_{s,i} u_{s',i^*} v_{s,j} v_{s',j^*}}_{\mathbb{E}_{u,v} [u_{s,i} u_{s',i^*} v_{s,j} v_{s',j^*}] = 0} + \mathbb{E} \underbrace{\sum_{i=i^*, j \neq j^*} \nabla f(W, \xi)_{i,j} \sum_{s,s'}^r \tau_s \tau_{s'} u_{s,i} u_{s',i} v_{s,j} v_{s',j^*}}_{\mathbb{E}_v [v_{s,j} v_{s',j^*}] = 0} \\ &\quad + \mathbb{E} \underbrace{\sum_{i \neq i^*, j=j^*} \nabla f(W, \xi)_{i,j} \sum_{s,s'}^r \tau_s \tau_{s'} u_{s,i} u_{s',i^*} v_{s,j} v_{s',j}}_{\mathbb{E}_u [u_{s,i} u_{s',i^*}] = 0} + \nabla f(W, \xi)_{i^*, j^*} \mathbb{E} \sum_{s,s'}^r \tau_s \tau_{s'} u_{s,i^*} u_{s',i^*} v_{s,j^*} v_{s',j^*} \\ &= \nabla f(W, \xi)_{i^*, j^*} \underbrace{\mathbb{E} \sum_{s \neq s'}^r \tau_s \tau_{s'} u_{s,i^*} u_{s',i^*} v_{s,j^*} v_{s',j^*}}_{\mathbb{E}_\tau [\tau_s \tau_{s'}] = 0} + \nabla f(W, \xi)_{i^*, j^*} \underbrace{\mathbb{E} \sum_{s=1}^r \tau_s^2 u_{s,i^*}^2 v_{s,j^*}^2}_{=r} = r \nabla f(W, \xi)_{i^*, j^*}. \end{aligned}$$

Clearly, when the SPSSA form is directly applied, the expectation of the TeZO gradient becomes r times the FO gradient. Therefore, by dividing r , TeZO is an unbiased estimation of the FO gradient.

Then we consider the variance. We have the following term:

$$\begin{aligned} \mathbb{E} \left\| \frac{1}{r} \lim_{\rho \rightarrow 0} \nabla^0 f(w, \xi) - \nabla f(W, \xi) \right\|^2 &= \frac{1}{r^2} \mathbb{E} \left\| \lim_{\rho \rightarrow 0} \nabla^0 f(w, \xi) \right\|^2 - \mathbb{E} \left\| \nabla f(W, \xi) \right\|^2 \\ &= \frac{1}{r^2} \mathbb{E} \left\| \left\langle \nabla f(W, \xi), \sum_{s=1}^r \tau_s \cdot (u_s \circ v_s) \right\rangle \cdot \sum_{s=1}^r \tau_s \cdot (u_s \circ v_s) \right\|^2 - \mathbb{E} \left\| \nabla f(W, \xi) \right\|^2 \end{aligned}$$

$$= \frac{1}{r^2} \mathbb{E} \left\langle \underbrace{\nabla f(W, \xi), \sum_{s=1}^r \tau_s \cdot (u_s \circ v_s)}_A \right\rangle^2 \cdot \left\langle \underbrace{\sum_{s=1}^r \tau_s \cdot (u_s \circ v_s), \sum_{s=1}^r \tau_s \cdot (u_s \circ v_s)}_B \right\rangle - \mathbb{E} \|\nabla f(W, \xi)\|^2.$$

Let $g_{ij} = \nabla f(W, \xi)_{i,j}$ for convenience, we have:

$$\begin{aligned} A &= \left\langle \nabla f(W, \xi), \sum_{s=1}^r \tau_s \cdot (u_s \circ v_s) \right\rangle^2 = \sum_{i,i'} \sum_{j,j'} \sum_{s,s'} g_{i,j} g_{i',j'} \tau_s \tau_{s'} u_{s,i} u_{s',i'} v_{s,j} v_{s',j'} \\ &= \underbrace{\sum_{i \neq i'} \sum_{j \neq j'} \sum_{s \neq s'} g_{i,j} g_{i',j'} \tau_s \tau_{s'} u_{s,i} u_{s',i'} v_{s,j} v_{s',j'}}_{A_1} + \underbrace{\sum_{i \neq i'} \sum_{j \neq j'} \sum_s g_{i,j} g_{i',j'} \tau_s^2 u_{s,i} u_{s,i'} v_{s,j} v_{s,j'}}_{A_2} \\ &\quad + \underbrace{\sum_{i \neq i'} \sum_j \sum_{s \neq s'} g_{i,j} g_{i',j} \tau_s \tau_{s'} u_{s,i} u_{s',i'} v_{s,j} v_{s',j}}_{A_3} + \underbrace{\sum_{i \neq i'} \sum_j \sum_s g_{i,j} g_{i',j} \tau_s^2 u_{s,i} u_{s,i'} v_{s,j} v_{s,j}}_{A_4} \\ &\quad + \underbrace{\sum_i \sum_{j \neq j'} \sum_{s \neq s'} g_{i,j} g_{i,j'} \tau_s \tau_{s'} u_{s,i} u_{s',i} v_{s,j} v_{s',j'}}_{A_5} + \underbrace{\sum_i \sum_{j \neq j'} \sum_s g_{i,j} g_{i,j'} \tau_s^2 u_{s,i} u_{s,i} v_{s,j} v_{s,j'}}_{A_6} \\ &\quad + \underbrace{\sum_i \sum_j \sum_{s \neq s'} g_{i,j}^2 \tau_s \tau_{s'} u_{s,i} u_{s',i} v_{s,j} v_{s',j}}_{A_7} + \underbrace{\sum_i \sum_j \sum_s g_{i,j}^2 \tau_s^2 u_{s,i}^2 v_{s,j}^2}_{A_8}. \end{aligned}$$

$$\begin{aligned} B &= \left\langle \sum_{s=1}^r \tau_s \cdot (u_s \circ v_s), \sum_{s=1}^r \tau_s \cdot (u_s \circ v_s) \right\rangle = \sum_i \sum_j \sum_{s,s'} \tau_s \tau_{s'} u_{s,i} u_{s',i} v_{s,j} v_{s',j} \\ &= \underbrace{\sum_i \sum_j \sum_{s \neq s'} \tau_s \tau_{s'} u_{s,i} u_{s',i} v_{s,j} v_{s',j}}_{B_1} + \underbrace{\sum_i \sum_j \sum_s \tau_s^2 u_{s,i}^2 v_{s,j}^2}_{B_2}. \end{aligned}$$

Similar to the way of computing expectations for the mean above, When there are cross terms like $u_{s,i}$ or $v_{s,j}$ in the product of A_i and B_j , then $\mathbb{E}_{u,v} [A_i B_j] = 0$. Therefore, it is easy to check that $\mathbb{E}_{u,v} [A_1 B] = \mathbb{E}_{u,v} [A_2 B] = \mathbb{E}_{u,v} [A_3 B] = \mathbb{E}_{u,v} [A_4 B] = \mathbb{E}_{u,v} [A_5 B] = \mathbb{E}_{u,v} [A_6 B] = 0$ and we have $\mathbb{E}_{u,v} [AB] = \mathbb{E}_{u,v} [(A_7 + A_8)(B_1 + B_2)]$. Then we consider the cross terms on τ_s . In $A_8 B_1$ and $A_7 B_2$, there exist the independent τ_s term, that is, $\mathbb{E}_\tau [A_8 B_1] = \mathbb{E}_\tau [A_7 B_2] = 0$, and the expectation of AB is $\mathbb{E}_{\tau,u,v} [AB] = \mathbb{E}_{\tau,u,v} [A_7 B_1 + A_8 B_2]$. For the first term, we have:

$$\mathbb{E} [A_7 B_1] = \mathbb{E} \left[2 \sum_i \sum_j \sum_{s \neq s'} g_{i,j}^2 \tau_s^2 \tau_{s'}^2 u_{s,i}^2 u_{s',i}^2 v_{s,j}^2 v_{s',j}^2 \right] = 2 \sum_i \sum_j \sum_{s \neq s'} g_{i,j}^2 = 2r(r-1) \sum_i \sum_j g_{i,j}^2.$$

For the second term, we have:

$$\begin{aligned} \mathbb{E} [A_8 B_2] &= \mathbb{E} \left[\sum_{i,i'} \sum_{j,j'} \sum_{s,s'} g_{i,j}^2 \tau_s^2 \tau_{s'}^2 u_{s,i}^2 u_{s',i'}^2 v_{s,j}^2 v_{s',j'}^2 \right] \\ &= \mathbb{E} \left[\sum_{i \neq i'} \sum_{j \neq j'} \sum_{s \neq s'} g_{i,j}^2 \tau_s^2 \tau_{s'}^2 u_{s,i}^2 u_{s',i'}^2 v_{s,j}^2 v_{s',j'}^2 \right] + \mathbb{E} \left[\sum_{i \neq i'} \sum_{j \neq j'} \sum_s g_{i,j}^2 \tau_s^4 u_{s,i}^2 u_{s',i'}^2 v_{s,j}^2 v_{s',j'}^2 \right] \\ &\quad + \mathbb{E} \left[\sum_{i \neq i'} \sum_j \sum_{s \neq s'} g_{i,j}^2 \tau_s^2 \tau_{s'}^2 u_{s,i}^2 u_{s',i'}^2 v_{s,j}^2 v_{s',j}^2 \right] + \mathbb{E} \left[\sum_{i \neq i'} \sum_j \sum_s g_{i,j}^2 \tau_s^4 u_{s,i}^2 u_{s',i'}^2 v_{s,j}^4 \right] \end{aligned}$$

$$\begin{aligned}
& + \mathbb{E} \left[\sum_i \sum_{j \neq j'} \sum_{s \neq s'} g_{i,j}^2 \tau_s^2 \tau_{s'}^2 u_{s,i}^2 u_{s',i}^2 v_{s,j}^2 v_{s',j'}^2 \right] + \mathbb{E} \left[\sum_i \sum_{j \neq j'} \sum_s g_{i,j}^2 \tau_s^4 u_{s,i}^4 v_{s,j}^2 v_{s,j'}^2 \right] \\
& + \mathbb{E} \left[\sum_i \sum_j \sum_{s \neq s'} g_{i,j}^2 \tau_s^2 \tau_{s'}^2 u_{s,i}^2 u_{s',i}^2 v_{s,j}^2 v_{s',j}^2 \right] + \mathbb{E} \left[\sum_i \sum_j \sum_s g_{i,j}^2 \tau_s^4 u_{s,i}^4 v_{s,j}^4 \right] \\
& = \sum_{i \neq i'} \sum_{j \neq j'} \sum_{s \neq s'} g_{i,j}^2 + \sum_{i \neq i'} \sum_{j \neq j'} \sum_s 3g_{i,j}^2 + \sum_{i \neq i'} \sum_j \sum_{s \neq s'} g_{i,j}^2 + \sum_{i \neq i'} \sum_j \sum_s 9g_{i,j}^2 \\
& + \sum_i \sum_{j \neq j'} \sum_{s \neq s'} g_{i,j}^2 + \sum_i \sum_{j \neq j'} \sum_s 9g_{i,j}^2 + \sum_i \sum_j \sum_{s \neq s'} g_{i,j}^2 + \sum_i \sum_j \sum_s 27g_{i,j}^2 \\
& = (mn r^2 + 2mn r + 6mr + 6nr + 12r) \sum_i \sum_j g_{i,j}^2.
\end{aligned}$$

Thus, we can consolidate all the results as follows:

$$\begin{aligned}
\mathbb{E} \left\| \frac{1}{r} \lim_{\rho \rightarrow 0} \nabla^0 f(w, \xi) - \nabla f(W, \xi) \right\|^2 &= \frac{1}{r^2} \mathbb{E} [A \cdot B] - \|\nabla f(W, \xi)\|^2 = \frac{1}{r^2} \mathbb{E} [A_7 B_1 + A_8 B_2] - \|\nabla f(W, \xi)\|^2 \\
&= \left(1 + mn + \frac{2mn}{r} + \frac{6(m+n)}{r} + \frac{10}{r} \right) \|\nabla f(W, \xi)\|^2.
\end{aligned}$$

This completes the proofs.

B.2. Proofs of Theorem 2

We first introduce some basic lemmas for the subsequent proofs. In fact, when considering the properties of the function at each layer, we treat the parameters and gradients as a 2D matrices. However, to consider its general property, we treat them as a flattened parameter vector concatenation across layers. Therefore, in our proof, we slightly abuse both uppercase and lowercase letters, e.g., $\nabla f(Z)$ and $\nabla f(z)$, to express the specific properties of the gradient.

Lemma 1. *Under Assumption 1 and 2, ZO gradient of T_{eZO} is an unbiased estimator of the full FO gradient $\nabla f(W)$ with the variance:*

$$\mathbb{E} \left\| \frac{1}{r} \nabla^0 f(W, \xi) - \nabla f(W) \right\|^2 \leq \rho^2 \lambda^2 \delta_\rho + (\delta + 1) \sigma^2 + \delta \mathbb{E} \|\nabla f(W)\|^2, \quad (12)$$

where $\delta = 1 + mn + \frac{2mn}{r} + \frac{6(m+n)}{r} + \frac{10}{r}$ and $\delta_\rho = \frac{15r^2(m+3)^3(n+3)^3 + 36r^2(r-1)m^3n^3 + r^2(r-1)(r-2)m^3n^3}{4}$ are two constants.

Proof. According to the studies of [Nesterov & Spokoiny \(2017\)](#); [Chen et al. \(2024\)](#); [Yu et al. \(2024\)](#), we first consider the smoothness property as follows:

$$f(W + \rho Z, \xi) - f(W, \xi) - \langle \nabla f(W, \xi), \rho Z \rangle \leq \frac{\lambda}{2} \|\rho Z\|^2 = \frac{\rho^2 \lambda}{2} \|Z\|^2.$$

Then we learn the distance between $\nabla^0 f(W)$ and the $\lim_{\rho \rightarrow 0} \nabla^0 f(W)$. Specifically, we consider the unbiased form as:

$$\begin{aligned}
& \left\| \frac{1}{r} \nabla^0 f(W, \xi) - \frac{1}{r} \lim_{\rho \rightarrow 0} \nabla^0 f(W, \xi) \right\|^2 \\
&= \frac{1}{r^2} \left\| \frac{f(W + \rho Z, \xi) - f(W - \rho Z, \xi)}{2\rho} \cdot Z - \langle \nabla f(W, \xi), Z \rangle \cdot Z \right\|^2 \\
&= \frac{1}{r^2} \left\| \frac{f(W + \rho Z, \xi) - f(W, \xi) + f(W, \xi) - f(W - \rho Z, \xi) - 2\langle \nabla f(W, \xi), \rho Z \rangle}{2\rho} \cdot Z \right\|^2 \\
&= \frac{1}{r^2} \left\| \frac{(f(W + \rho Z, \xi) - f(W, \xi) - \langle \nabla f(W, \xi), \rho Z \rangle) - (f(W - \rho Z, \xi) - f(W, \xi) - \langle \nabla f(W, \xi), -\rho Z \rangle)}{2\rho} \right\|^2 \cdot \|Z\|^2 \\
&\leq \frac{\rho^2 \lambda^2}{4r^2} \|Z\|^6.
\end{aligned}$$

Substituting $Z = \sum_{s=1}^r \tau_s \cdot u_s \circ v_s$ and taking the expectation, we have:

$$\begin{aligned} \mathbb{E} \left\| \frac{1}{r} \nabla^0 f(W, \xi) - \frac{1}{r} \lim_{\rho \rightarrow 0} \nabla^0 f(W, \xi) \right\|^2 &\leq \frac{\rho^2 \lambda^2}{4r^2} \mathbb{E} \|Z\|^6 = \frac{\rho^2 \lambda^2}{4r^2} \mathbb{E} \left\| \sum_{s=1}^r \tau_s \cdot u_s \circ v_s \right\|^6 \\ &= \frac{\rho^2 \lambda^2}{4r^2} \mathbb{E} \left(\left\| \sum_{s=1}^r \tau_s \cdot u_s \circ v_s \right\|^2 \right)^3 \leq \frac{\rho^2 \lambda^2}{4r^2} \mathbb{E} \left(r \sum_{s=1}^r \tau_s^2 \|u_s \circ v_s\|^2 \right)^3 = \frac{r \rho^2 \lambda^2}{4} \mathbb{E} \left(\sum_{s=1}^r \tau_s^2 \|u_s\|^2 \|v_s\|^2 \right)^3. \end{aligned}$$

Similarly, we can expand the term as:

$$\begin{aligned} \mathbb{E} \left(\sum_{s=1}^r \tau_s^2 \|u_s\|^2 \|v_s\|^2 \right)^3 &= \mathbb{E} \sum_s \sum_{s'} \sum_{s''} \tau_s^2 \tau_{s'}^2 \tau_{s''}^2 \|u_s\|^2 \|u_{s'}\|^2 \|u_{s''}\|^2 \|v_s\|^2 \|v_{s'}\|^2 \|v_{s''}\|^2 \\ &= \mathbb{E} \sum_s \sum_{s'=s} \sum_{s''=s'} \tau_s^6 \|u_s\|^6 \|v_s\|^6 + \mathbb{E} \sum_s \sum_{s'=s} \sum_{s'' \neq s'} \tau_s^4 \tau_{s''}^2 \|u_s\|^4 \|u_{s''}\|^2 \|v_s\|^4 \|v_{s''}\|^2 \\ &\quad + \mathbb{E} \sum_s \sum_{s' \neq s} \sum_{s''=s} \tau_s^4 \tau_{s'}^2 \|u_s\|^4 \|u_{s'}\|^2 \|v_s\|^4 \|v_{s'}\|^2 + \mathbb{E} \sum_s \sum_{s' \neq s} \sum_{s'' \neq s'} \tau_s^2 \tau_{s'}^4 \|u_s\|^2 \|u_{s'}\|^4 \|v_s\|^2 \|v_{s'}\|^4 \\ &\quad + \mathbb{E} \sum_s \sum_{s' \neq s} \sum_{s'' \neq s, s'} \tau_s^2 \tau_{s'}^2 \tau_{s''}^2 \|u_s\|^2 \|u_{s'}\|^2 \|u_{s''}\|^2 \|v_s\|^2 \|v_{s'}\|^2 \|v_{s''}\|^2. \end{aligned}$$

Then we will discuss each term one by one. Actually, since τ, u, v are independent from each other, the expectation can be separated term by term. Since $u_s \sim \mathcal{N}(0, I_m)$, $v_s \sim \mathcal{N}(0, I_n)$ and $\tau_s \sim \mathcal{N}(0, 1)$, we have: $\mathbb{E} \|u_s\|^2 = m$, $\mathbb{E} \|u_s\|^4 = m(2m-1) \leq 2m^2$, $\mathbb{E} \|u_s\|^6 = m(15+3(m-1)+(m-1)(m-2)) \leq (m+3)^3$, $\mathbb{E} \|v_s\|^2 = n$, $\mathbb{E} \|v_s\|^4 = n(2n-1) \leq 2n^2$, $\mathbb{E} \|v_s\|^6 = n(15+3(n-1)+(n-1)(n-2)) \leq (n+3)^3$, $\mathbb{E} [\tau_s^2] = 1$, $\mathbb{E} [\tau_s^4] = 3$ and $\mathbb{E} [\tau_s^6] = 15$. Therefore, we can provide the upper bound:

$$\mathbb{E} \left(\sum_{s=1}^r \tau_s^2 \|u_s\|^2 \|v_s\|^2 \right)^3 \leq 15r(m+3)^3(n+3)^3 + 36r^2m^3n^3 + r^3m^3n^3.$$

Let $\delta_\rho = \frac{15r^2(m+3)^3(n+3)^3 + 36r^3m^3n^3 + r^4m^3n^3}{4}$, then we have:

$$\mathbb{E} \left\| \frac{1}{r} \nabla^0 f(W, \xi) - \frac{1}{r} \lim_{\rho \rightarrow 0} \nabla^0 f(W, \xi) \right\|^2 \leq \frac{r \rho^2 \lambda^2}{4} \mathbb{E} \left(\sum_{s=1}^r \tau_s^2 \|u_s\|^2 \|v_s\|^2 \right)^3 \leq \rho^2 \lambda^2 \delta_\rho.$$

Combining it with the variance in Theorem 1, we can finish the proofs. \square

Then we can easily solve the convergence for TeZO. Similarly, without loss of generality, we still consider the 2D parameters. Let $\eta \leq \frac{1}{\lambda(\delta+1)}$. By expanding the smoothness inequality, we have:

$$\begin{aligned} \mathbb{E}_t [f(W_{t+1})] &\leq f(W_t) + \mathbb{E}_t \langle \nabla f(W_t), W_{t+1} - W_t \rangle + \frac{\lambda}{2} \mathbb{E}_t \|W_{t+1} - W_t\|^2 \\ &= f(W_t) + \eta \mathbb{E}_t \langle \nabla f(W_t), -G_t \rangle + \frac{\lambda \eta^2}{2} \mathbb{E}_t \|G_t\|^2 \\ &= f(W_t) - \eta \mathbb{E}_t \|\nabla f(W_t)\|^2 + \frac{\lambda \eta^2}{2} \mathbb{E}_t \|G_t\|^2 \\ &\leq f(W_t) - \eta \mathbb{E}_t \|\nabla f(W_t)\|^2 + \frac{\lambda \eta^2}{2} \mathbb{E}_t \left\| \frac{1}{r} \nabla^0 f(W_t, \xi) - \nabla f(W_t) \right\|^2 + \frac{\lambda \eta^2}{2} \mathbb{E}_t \|\nabla f(W_t)\|^2 \\ &\leq f(W_t) - \eta \left(1 - \frac{\lambda(1+\delta)\eta}{2} \right) \mathbb{E}_t \|\nabla f(W_t)\|^2 + \eta^2 \rho^2 \frac{\lambda^3 \delta_\rho}{2} + \eta^2 \frac{\lambda(\delta+1)\sigma^2}{2} \\ &\leq f(W_t) - \frac{\eta}{2} \mathbb{E}_t \|\nabla f(W_t)\|^2 + \eta^2 \rho^2 \frac{\lambda^3 \delta_\rho}{2} + \eta^2 \frac{\lambda(\delta+1)\sigma^2}{2}. \end{aligned}$$

Therefore, let $D_0 = f(W_0) - f(W_*)$ be the initialized bias where W_* is the optimal solution, by accumulating it from $t = 0$ to $T - 1$ and taking the full expectation, we have:

$$\frac{1}{T} \sum_{t=0}^{T-1} \mathbb{E} \|\nabla f(W_t)\|^2 \leq \frac{2D_0}{\eta T} + \eta \lambda (\rho^2 \lambda^2 \delta_\rho + (\delta + 1) \sigma^2).$$

By simply selecting the learning rate $\eta = \mathcal{O} \left(\sqrt{\frac{D_0}{\lambda T (\rho^2 \lambda^2 \delta_\rho + \delta \sigma^2)}} \right) \leq \frac{1}{\lambda(\delta+1)}$, we have:

$$\frac{1}{T} \sum_{t=0}^{T-1} \mathbb{E} \|\nabla f(W_t)\|^2 = \mathcal{O} \left(\sqrt{\frac{\lambda D_0 (\rho^2 \lambda^2 \delta_\rho + \delta \sigma^2)}{T}} \right).$$